

CACHD1 is an $\alpha 2\delta$ -like protein that modulates CaV3 voltage-gated calcium channel activity

Article

Accepted Version

Cottrell, G. S. ORCID: <https://orcid.org/0000-0001-9098-7627>, Soubrane, C. H., Hounshell, J. A., Lin, H., Owenson, V., Rigby, M., Cox, P. J., Barker, B. S., Ottolini, M., Ince, S., Bauer, C. C., Perez-Reyes, E., Patel, M. K., Stevens, E. B. and Stephens, G. J. ORCID: <https://orcid.org/0000-0002-8966-4238> (2018) CACHD1 is an $\alpha 2\delta$ -like protein that modulates CaV3 voltage-gated calcium channel activity. The Journal of Neuroscience, 38 (4). pp. 9186-9201. ISSN 1529-2401 doi: 10.1523/JNEUROSCI.3572-15.2018 Available at <https://centaur.reading.ac.uk/79082/>

It is advisable to refer to the publisher's version if you intend to cite from the work. See [Guidance on citing](#).

To link to this article DOI: <http://dx.doi.org/10.1523/JNEUROSCI.3572-15.2018>

Publisher: The Society for Neuroscience

All outputs in CentAUR are protected by Intellectual Property Rights law, including copyright law. Copyright and IPR is retained by the creators or other copyright holders. Terms and conditions for use of this material are defined in

the [End User Agreement](#).

www.reading.ac.uk/centaur

CentAUR

Central Archive at the University of Reading

Reading's research outputs online

Research Articles: Cellular/Molecular

CACHD1 is an $\alpha 2\delta$ -like protein that modulates Cav3 voltage-gated calcium channel activity

Graeme S. Cottrell¹, Camille H. Soubrane¹, James A. Hounshell^{3,5}, Hong Lin¹, Venetia Owenson², Michael Rigby², Peter J. Cox², Bryan S. Barker^{3,5}, Matteo Ottolini³, Selvi Ince¹, Claudia C. Bauer¹, Edward Perez-Reyes^{4,5}, Manoj K. Patel^{3,5}, Edward B. Stevens² and Gary J. Stephens¹

¹University of Reading, Whiteknights Campus, Reading, RG6 6AJ.

²Pfizer Neuroscience and Pain Research Unit, Portway Building, Granta Park, Great Abington, Cambridge, CB21 6GS.

³Departments of Anesthesiology

⁴Pharmacology

⁵Neuroscience Graduate Program, University of Virginia, Charlottesville, VA, USA, 22908

DOI: 10.1523/JNEUROSCI.3572-15.2018

Received: 22 September 2015

Revised: 3 June 2018

Accepted: 13 June 2018

Published: 4 September 2018

Author contributions: G.S.C., C.H.S., J.H., P.C., E.P.-R., M.K.P., E.B.S., and G.J.S. designed research; G.S.C., C.H.S., J.H., H.L., V.O., B.S.B., M.O., S.I., C.b., and M.K.P. performed research; G.S.C., C.H.S., J.H., H.L., M.R., B.S.B., and M.K.P. analyzed data; C.H.S., M.K.P., E.B.S., and G.J.S. wrote the paper; P.C., E.P.-R., E.B.S., and G.J.S. contributed unpublished reagents/analytic tools.

Conflict of Interest: The authors declare no competing financial interests.

Work supported by a BBSRC Departmental Training Grant award with CASE award from Pfizer UK to GJS and EBS to support CHS. This work was also supported by NIH/NINDS grant NS075157 to MKP and NIH grant NS069524 to EPR.

Corresponding authors: Gary J. Stephens, School of Pharmacy, University of Reading, Whiteknights, PO Box 228, Reading RG6 6AJ, UK. E-mail: g.j.stephens@reading.ac.uk Edward B Stevens, Pfizer Neuroscience and Pain Research Unit, Portway Building, Granta Park, Cambridge, CB21 6GS, UK. Email: edward.stevens@metrionbiosciences.com.

Cite as: J. Neurosci ; 10.1523/JNEUROSCI.3572-15.2018

Alerts: Sign up at www.jneurosci.org/cgi/alerts to receive customized email alerts when the fully formatted version of this article is published.

Accepted manuscripts are peer-reviewed but have not been through the copyediting, formatting, or proofreading process.

Copyright © 2018 the authors

CACHD1 is an $\alpha 2\delta$ -like protein that modulates Ca_v3 voltage-gated calcium channel activity

Abbreviated title: CACHD1 modulation of Ca_v3 channels

Graeme S. Cottrell^{1*}, Camille H. Soubrane^{1*}, James A. Hounshell^{3,5}, Hong Lin¹, Venetia Owenson², Michael Rigby², Peter J. Cox², Bryan S. Barker^{3,5}, Matteo Ottolini³, Selvi Ince¹, Claudia C. Bauer¹, Edward Perez-Reyes^{4,5}, Manoj K. Patel^{3,5}, Edward B. Stevens², Gary J. Stephens¹

¹University of Reading, Whiteknights Campus, Reading, RG6 6AJ.

²Pfizer Neuroscience and Pain Research Unit, Portway Building, Granta Park, Great Abington, Cambridge, CB21 6GS.

Departments of ³Anesthesiology, ⁴Pharmacology, and ⁵Neuroscience Graduate Program, University of Virginia, Charlottesville, VA, USA, 22908.

*These authors contributed equally to this work.

Corresponding authors:

Gary J. Stephens, School of Pharmacy, University of Reading, Whiteknights, PO Box 228, Reading RG6 6AJ, UK. E-mail: g.j.stephens@reading.ac.uk.

Edward B Stevens, Pfizer Neuroscience and Pain Research Unit, Portway Building, Granta Park, Cambridge, CB21 6GS, UK. Email: edward.stevens@metrionbiosciences.com.

Number of pages: 46

Number of figures: 9; tables: 2

Number of words for Abstract (191), Introduction (429), and Discussion (1561)

26 **Acknowledgements**

27 Work supported by a BBSRC Departmental Training Grant award with CASE award from
28 Pfizer UK to GJS and EBS to support CHS. This work was also supported by NIH/NINDS
29 grant NS075157 to MKP and NIH grant NS069524 to EPR.

30
31 **Abstract**

32 The putative cache (Ca^{2+} channel and chemotaxis receptor) domain containing 1 (CACHD1)
33 protein has predicted structural similarities to members of the $\alpha 2\delta$ voltage-gated Ca^{2+} channel
34 (VGCC) auxiliary subunit family. CACHD1 mRNA and protein were highly expressed in the
35 male mammalian CNS, in particular in the thalamus, hippocampus and cerebellum, with a
36 broadly similar tissue distribution to Ca_v3 subunits, in particular, $\text{Ca}_v3.1$. In expression
37 studies, CACHD1 increased cell-surface localization of $\text{Ca}_v3.1$ and these proteins were in
38 close proximity at the cell surface consistent with the formation of CACHD1- $\text{Ca}_v3.1$
39 complexes. In functional electrophysiological studies, co-expression of human CACHD1
40 with $\text{Ca}_v3.1$, $\text{Ca}_v3.2$ and $\text{Ca}_v3.3$ caused a significant increase in peak current density and
41 corresponding increases in maximal conductance. By contrast, $\alpha 2\delta-1$ had no effect on peak
42 current density or maximal conductance in either $\text{Ca}_v3.1$, $\text{Ca}_v3.2$ or $\text{Ca}_v3.3$. Comparison of
43 CACHD1-mediated increases in $\text{Ca}_v3.1$ current density and gating currents revealed an
44 increase in channel open probability. In hippocampal neurons from male and female E19 rats,
45 CACHD1 overexpression increased Ca_v3 -mediated action potential (AP) firing frequency
46 and neuronal excitability. These data suggest that CACHD1 is structurally an $\alpha 2\delta$ -like
47 protein that functionally modulates Ca_v3 voltage-gated calcium channel activity.

48
49

50 **Significance Statement**

51 This is the first study to characterise the CACHD1 protein. CACHD1 is widely expressed in
52 the CNS, in particular in the thalamus, hippocampus and cerebellum. CACHD1 distribution
53 is similar to that of low-voltage-activated (Cav3, T-type) calcium channels, in particular to
54 Cav3.1, a protein which regulates neuronal excitability and is a potential therapeutic target in
55 conditions such as epilepsy and pain. CACHD1 is structurally a $\alpha 2\delta$ -like protein that
56 functionally increases Cav3 calcium current. CACHD1 increases the presence of Cav3.1 at
57 the cell surface, forms complexes with Cav3.1 at the cell-surface and causes an increase in
58 channel open probability. In hippocampal neurons, CACHD1 causes increases in neuronal
59 firing. Thus, CACHD1 represents a novel protein that modulates Cav3 activity.

60

61

62

63 **Introduction**

64 The putative CACHD1 gene was identified following a systematic search for proteins with
 65 structural homology to $\alpha 2\delta$ VGCC auxiliary subunits. The human CACHD1 gene on
 66 chromosome 1p31.3 encodes the putative protein CACHD1 and has many orthologs,
 67 including in speciation as early as *C. elegans* (tag-180) and *D. melanogaster* (CG16868)
 68 (Anantharaman and Aravind, 2000). Despite only a 13-16% gene homology and a <21%
 69 protein identity with the $\alpha 2\delta$ VGCC auxiliary subunits, there are several key structural
 70 similarities between CACHD1 and $\alpha 2\delta$ in terms of the arrangement of protein motifs. $\alpha 2\delta$
 71 and $\text{Cav}\beta$ subunits are described as auxiliary or accessory VGCC subunits that modulate cell-
 72 surface expression and biophysical properties of high-voltage-activated (HVA) $\text{Cav}1$ (L-type
 73 Ca^{2+} current) and $\text{Cav}2$ (P/Q, N- and R-type Ca^{2+} current) VGCC major $\alpha 1$ subunits
 74 (Dolphin, 2012; Dolphin, 2013). In particular, $\alpha 2\delta$ subunits are proposed to associate with
 75 HVA channels within the secretory pathway to promote plasma membrane trafficking and,
 76 consequentially, to contribute to synaptic abundance (Dolphin, 2012), transmitter release
 77 (Hoppa et al., 2012) and to defining the extent of the active zone (Schneider et al., 2015).
 78 $\alpha 2\delta$ -1 and $\alpha 2\delta$ -2 represent molecular targets of gabapentinoid drugs (Dooley et al., 2007).
 79 However, modulation of low-voltage-activated (LVA) $\text{Cav}3$ family (T-type Ca^{2+} current) by
 80 existing $\alpha 2\delta$ and $\text{Cav}\beta$ auxiliary subunits has not been firmly established (Dolphin et al.,
 81 1999; Lacinová et al., 1999; Dubel et al., 2004). LVA currents are activated by small
 82 depolarization to regulate excitability around the resting membrane potential and $\text{Cav}3$
 83 channels have been proposed as therapeutic targets in diseases such as epilepsy and pain
 84 (Perez-Reyes, 2003; Cheong and Shin, 2013; Powell et al., 2014; Snutch and Zamponi,
 85 2017); therefore, knowledge of proteins that modulate $\text{Cav}3$ activity is paramount.

86 Here, we investigate the novel CACHD1 protein and test the hypothesis that
87 CACHD1 represents an $\alpha 2\delta$ -like protein that modulates Ca_v3 channels. We have previously
88 reported that, by contrast to $\alpha 2\delta$, the CACHD1 subunit has no clear effect on $\text{Ca}_v2.2$
89 biophysical properties when co-expressed together with $\beta 2a$ in expression system studies
90 (Soubrane *et al.*, 2012). We characterise the expression of the CACHD1 gene in rat and
91 human tissue at the transcriptional and translational level, and demonstrate that CACHD1,
92 but not $\alpha 2\delta$ -1, increases Ca_v3 (T-type) current density and maximal conductance. CACHD1
93 increases $\text{Ca}_v3.1$ channel levels at the plasma membrane and data were consistent with
94 CACHD1 forming complexes with $\text{Ca}_v3.1$ at the cell surface to increase channel open
95 probability. We further demonstrate that CACHD1 expression causes a functional increase in
96 T-type current-mediated excitability in hippocampal neurons. Together, these data
97 demonstrate that CACHD1 is structurally an $\alpha 2\delta$ -like protein which functionally modulates
98 Ca_v3 activity.
99

100 **Materials and Methods**

101

102 **RNA isolation and real-time polymerase chain reaction (PCR)**

103 Tissue samples were dissected from 5 adult male Wistar rats (Harlan, UK) following
 104 isoflurane overdose and cervical dislocation, according to Home Office Animals (Scientific
 105 procedures) Act 1986, UK. Total RNA was extracted using an RNeasy kit (Qiagen, UK) with
 106 an on-column DNase I treatment. Additional total RNA samples from AMS Biotechnology
 107 (Abingdon, UK) originated from human male donors aged 24-65. RNA (500 ng) was reverse-
 108 transcribed and relative quantification of CACHD1 and $\alpha 2\delta$ -1 transcripts was performed
 109 using SYBR green and custom-made validated primers. HPRT1 was used as housekeeping
 110 gene. Absolute quantification of CACHD1, $\alpha 2\delta$ -1, -2, -3, $Ca_v2.2$ and Ca_v1 , -2, -3 transcripts
 111 was evaluated using 'Best Coverage' Taqman probes (Applied Biosystems, UK) against a
 112 standard curve of plasmids containing human CACHD1 and a rat single stranded DNA
 113 standard curve.

114

115 **Sample preparation for *in situ* hybridization and immunohistochemistry**

116 Rat tissue was kindly donated by Dr Emilio Russo, University Magna Grecia of Catanzaro,
 117 Italy. Briefly, 6-month-old male rats were sacrificed by i.p. injection of pentobarbital (200
 118 mg/kg) according to ARRIVE guidelines and local ethical approval committee of the
 119 University of Catanzaro and perfused-fixed with 4% PFA in RNase-free PBS, pH 7.3. Brain
 120 tissue was extracted, post-fixed overnight in 4% PFA in RNase-free PBS and then
 121 cryoprotected in 30% sucrose. After being processed to wax (Tissue-tek VIP), 5 μ m
 122 horizontal plane brain slices were cut using a microtome (Leica, UK).

123

124 ***In situ* hybridization**

125 A CACHD1 probe consisting of a cocktail of short 10-20bp oligonucleotides spanning ~1kb
 126 was designed by ACDBio (USA) and *in situ* hybridization was performed on 5 µm rat brain
 127 sections using a RNAscope 2.0 FFPE-Red kit. Positive (POLR2A) and negative (DapB)
 128 probes were run in parallel.

129

130 **Immunohistochemistry**

131 Chromogenic immunohistochemistry was performed using antigen retrieval in citrate buffer
 132 (Thermo, UK) for 10 min and 3,3'-diaminobenzidine (DAB) staining (ImmPACT, Vector
 133 Labs, UK), dehydrated and mounted with DPX. Rabbit anti-CACHD1 (1:500) (Abcam, UK
 134 Cat #AB75141, RRID: AB_1310016) with horseradish peroxidase-coupled anti-rabbit IgG
 135 (ImmPRESS, Vector Labs, UK) was used to detect CACHD1 protein. Qualitative expression
 136 of mRNA was evaluated with a brightfield microscope according to colour intensity of
 137 labelled mRNA.

138

139 **Antibodies for biochemistry**

140 The following antibodies were used: mouse anti-HA.11 (Cambridge Bioscience, UK; clone
 141 16B12; Lot No. B220767, RRID: AB_10063630); rabbit anti-Na⁺/K⁺-ATPase (Novus
 142 Biologicals, Abingdon, UK; NB100-80005, Lot No. YH02206, RRID: AB_2063297); mouse
 143 anti-c-Myc (Sigma-Aldrich Cat# M4439, clone 9E10, Lot No. 087M4765V, RRID:
 144 AB_439694), rabbit anti-c-Myc (Sigma-Aldrich Cat# C3956, Lot No. 016M4762V, RRID:
 145 AB_439680), mouse anti-β-actin (Sigma-Aldrich Cat# A5441, Lot No. 028K4826, RRID:
 146 AB_476744) and rabbit anti-CACHD1 (Sigma-Aldrich Cat# AV49592, Lot No. QC22258,
 147 RRID: AB_1852421); goat anti-mouse or rabbit IgG coupled to horseradish peroxidase

148 (Strattech Scientific Limited, Newmarket, UK); donkey anti-mouse or rabbit coupled to
 149 AlexaFluor488, 555 or 647 (Invitrogen, Paisley, UK). Note: We experienced vial-to-vial
 150 variation with the rabbit anti-CACHD1 antibody for Western blotting during this study.
 151 Although both vials were from the same Lot No. and specifically recognised CACHD1, the
 152 vial used for Fig. 4D gave rise to more non-specific staining on HEK cell lysates than vial
 153 used for Fig. 4A.

154 **Vectors and vector construction**

156 The human CACHD1 construct was purchased from Origene (Rockville, MA, USA) and the
 157 truncated clone completed by PCR. The subsequent open reading frame was then subcloned
 158 into pcDNA5/FRT. An N-terminal Myc tag was inserted after the natural signal sequence
 159 between Ala³⁵-Glu³⁶ using standard PCR techniques. All constructs were sequenced to
 160 confirm identity. Construction of the vector pcDNA5/FRT-HA-CLR-Myc-RAMP1 has been
 161 described elsewhere (Cottrell et al., 2007).

162 **Cell maintenance and propagation**

164 HEK293 tsA201 (HEK) cells were cultured in DMEM (Invitrogen, UK) containing 10% fetal
 165 bovine serum (Biosera, UK) and maintained in 95% air, 5% CO₂ at 37 °C.

166 **Cell-surface biotinylation**

168 HEK cells were transiently transfected in 6 well plates using 3 µg DNA (ratio 2:1, GFP-
 169 Cav3.1-HA:CACHD1) using Lipofectamine²⁰⁰⁰ (3:8, DNA:Lipofectamine²⁰⁰⁰). HEK cells
 170 transfected with empty vector (vector control, VC), VC + Myc-CACHD1, GFP-Cav3.1-HA +
 171 VC or GFP-Cav3.1-HA + Myc-CACHD1 were washed (3x PBS), incubated with 0.3 mg/ml

172 EZ-Link™-Sulfo-NHS-Biotin (Pierce, USA) in PBS (1 h, 4°C), washed (3x PBS) and cells
 173 lysed in RIPA buffer (50 mM Tris/HCl, pH 7.4, 150 mM NaCl, 5 mM MgCl₂, 1 mM EGTA,
 174 10 mM NaF, 10 mM Na₄P₂O₇, 0.1 mM Na₃VO₄, 0.5% Nonidet P-40, peptidase inhibitor
 175 cocktail (Roche, UK)), and centrifuged. Biotinylated proteins were recovered by incubation
 176 with NeutrAvidin-agarose (30 µl, overnight, 4°C), pelleted, washed with RIPA buffer (3x 1
 177 ml), boiled in Laemmli buffer and analyzed by SDS-PAGE and Western blotting.

178 **SDS-PAGE and Western blotting**

180 Immunoprecipitations and whole cell lysates were separated by SDS-PAGE (6-9%
 181 acrylamide), proteins transferred to PVDF membranes (Immobilon-P, Millipore, UK) and
 182 blocked for 1 h at room temperature (1x PBS, 0.1% Tween²⁰, 5% non-fat milk powder
 183 [blocking buffer]). Membranes were incubated with antibodies to HA (1:5,000), β-actin
 184 (1:20,000), CACHD1 (1:1000), rabbit or mouse Myc (1:5000) or Na⁺-K⁺-ATPase (1:20,000)
 185 (overnight, 4°C; blocking buffer). Membranes were washed for 30 min (1x PBS, 0.1%
 186 Tween²⁰) and incubated with appropriate secondary antibodies coupled to horseradish
 187 peroxidase (1:10,000, 1 h, room temperature; blocking buffer). Immunoreactive proteins were
 188 detected using enhanced chemiluminescence (BioRad, UK). Densitometric analysis was
 189 performed using an ImageQuant-RT ECL imaging system (GE Healthcare, Chalfont St Giles,
 190 UK) and analysed using ImageQuant TL software.

191 **Immunofluorescent detection of cell-surface proteins**

193 HEK cells were transiently transfected in 12 well plates using 1 µg DNA (ratio 2:1, GFP-
 194 Cav3.1-HA:Myc-CACHD1) using polyethylenimine (PEI; 1:2, DNA:PEI). HEK cells
 195 transfected with empty vector (vector control, VC), VC + Myc-CACHD1, GFP-Cav3.1-HA +

196 VC, GFP-Cav3.1-HA + Myc-CACHD1 or CLR•RAMP1 seeded onto coverslips and used for
 197 experimentation after 48 h. Cells were washed twice with PBSCM, incubated in DMEM
 198 containing 0.1% BSA and mouse anti-HA (1:100) and rabbit anti-c-Myc (1:500) antibodies
 199 (1 h, 4°C), washed twice again with PBSCM and then fixed in 100 mM PBS containing 4%
 200 paraformaldehyde (w/v), pH 7.4 (20 min, 4°C). Coverslips were incubated in blocking buffer
 201 (1x PBS, 2% normal horse serum, 0.1% saponin) (30 min, room temperature (RT)) and then
 202 incubated with appropriate secondary antibodies (1:2000, 2 h, RT). Coverslips were washed
 203 (blocking buffer, 30 min, RT) and mounted using Vectashield containing DAPI.

204

205 **Proximity ligation assays**

206 HEK cells were transiently transfected in 12 well plates using 1 µg DNA (ratio 2:1, GFP-
 207 Cav3.1-HA:Myc-CACHD1) using polyethylenimine (PEI; 1:2, DNA:PEI). HEK cells
 208 transfected with empty vector (vector control, VC), VC + Myc-CACHD1, GFP-Cav3.1-HA +
 209 VC, GFP-Cav3.1-HA + Myc-CACHD1 or CLR•RAMP1 seeded onto coverslips and used for
 210 experimentation after 48 h. Cells were washed twice with PBSCM, incubated in DMEM
 211 containing 0.1% BSA and mouse anti-HA (1:100) and rabbit anti-c-Myc (1:500) antibodies
 212 (1 h, 4°C), washed twice again with PBSCM and then fixed in 100 mM PBS containing 4%
 213 paraformaldehyde (w/v), pH 7.4 (20 min, 4°C). After washing with PBSCM the proximity
 214 ligation assay was conducted according to the manufacturer's instructions (Duolink® In Situ
 215 Red Starter Kit Mouse/Rabbit, Cat No. DUO92101, Sigma). Briefly, cells were blocked (1 h,
 216 37°C), washed twice (5 min, room temperature) and then incubated with appropriate
 217 secondary antibodies (1 h, 37°C). After washing (2x 5 min, room temperature), the ligation
 218 was conducted (30 min, 37°C) and the cells were washed twice more. Coverslips were then

219 incubated with the amplification reaction mixture (100 min, 37°C), washed and coverslips
220 mounted in medium containing DAPI.

221

222 **Confocal microscopy**

223 Cells were observed with a Nikon Eclipse Ti laser-scanning confocal microscope using a
224 100x/1.45 Oil DIC N2 objective. Images were collected at a zoom of 1-2 and at least five
225 optical sections were taken at intervals of 0.5 μ m. Single sections are shown. Images were
226 processed using Adobe Photoshop and the NIS-Elements AR software.

227

228 **Transformed human embryonic kidney cell culture and transfection for** 229 **electrophysiology**

230 For electrophysiology experiments, HEK cells were transfected using 4 μ l Fugene6
231 (Promega, UK) with total 2 μ g pcDNA3 at 50:1:25 for Cav3.1/pmaxGFP, Cav3.2/pmaxGFP
232 or Cav3.3/pmaxGFP with or without α 2 δ -1 or CACHD1. Empty vector was used to
233 compensate when α 2 δ or CACHD1 was omitted. Cells were maintained at 95% air, 5% CO₂
234 at 37 °C and used for experimentation 24-48 h post transfection.

235

236 **Hippocampal neuron culture and transfection**

237 Low-density hippocampal cultures were prepared from male and female E19 rat embryos as
238 described previously (Zhang et al., 2003). All experiments were carried out in compliance
239 with the Guide for the Care and Use of Laboratory Animals of the National Institutes of
240 Health and approved by the University of Virginia Animal Care and Use Committee and
241 adhered to ARRIVE guidelines. Neurons were plated onto poly-L-lysine coated glass
242 coverslips at a density of \sim 70 cells/mm² and were transfected using lipofectamine 2000 at a

ratio of 2 μ l lipofectamine 2000 per 1 μ g DNA. Neurons were transfected with either CACHD1 or pcDNA3.1 at a ratio of 10:1 excess to mVenus and moved 24 h after transfection to a new glia-feeder layer.

Electrophysiology

Recordings from HEK cells were made as described previously (Vogl et al., 2015). Current-voltage (I-V) relationships from individual cells were fitted with a modified Boltzmann equation: $I = G_{\max} \times (V - V_{\text{rev}}) / (1 + \exp(-(V - V_{1/2})/k))$ where, G_{\max} is the maximal conductance (nS/pF), $V_{1/2}$ is the midpoint of activation i.e. the voltage at which 50% of the channels are open, V_{rev} is the null potential and k is the slope factor. Tail currents (measured at -120 mV) were normalised to the maximal and minimal conductance and the resultant curves were fitted with following Boltzmann function: $I = I_0 + ((I_{\max} - I_0) / (1 + \exp((V_{1/2} - V)/k)))$. Throughout, all comparative electrophysiological experiments were performed in transfection-matched cultures.

Recordings from hippocampal neurons were performed as described previously (Jones et al., 2007). Throughout, data are expressed as mean S.E.M. Methods to estimate the probability of channel opening, P_o have been previously described by us (Shcheglovitov et al., 2008), which assumes no change in single channel current, reducing the relationship between whole-cell current (I) to $I \approx NP_o$, where N is the number of channels in a cell and P_o is the probability of channel opening. N is estimated by measuring the channel gating current at the reversal potential for ionic current. The peak current represents the maximal gating charge Q_{\max} , and is proportional to N . Peak ionic current conductance, G_{\max} , was determined by fitting the I-V curve, obtained from the same cell, with a Boltzmann-Ohm equation as

266 described earlier. G_{\max} is used as a proxy for I since it is not affected by changes in driving
267 force. Therefore, the G_{\max}/Q_{\max} ratio can be used to estimate P_o .

268

269 **Experimental Design and Statistical Analysis**

270 Throughout, all animal studies comply to appropriate ARRIVE and NIH guidelines and
271 comply to country and institute guidelines (as specified in Methods section for each animal
272 study). Details of animal strain, sex and method of sacrifice and use of anaesthetics are also
273 stated in Methods section for each animal study.

274

275 Throughout, all comparative biochemical and electrophysiological experiments were
276 performed against transfection-matched culture controls. For electrophysiological
277 experiments in recombinant cells, a minimum of 5 separate transfections were performed and
278 numbers of individual replications are specified in appropriate Table. In all cases, sample size
279 is stated in text, Figure legend or appropriate Table. Data subjected to statistical comparisons
280 were assessed for assumptions of normality using a D'Agostino-Pearson omnibus test and
281 expressed as mean \pm standard error of the mean (SEM) throughout. Groups were compared
282 by two-tailed paired or unpaired Student's t -test, Mann-Whitney test, one- or two-way
283 ANOVA tests followed by Bonferroni post-hoc tests, Kruskal-Wallis test and Dunn's
284 multiple comparison test or least squares fits compared using extra sum of squares F test as
285 appropriate, using GraphPad Prism. In all cases, the statistical test used is stated in text,
286 Figure legend or appropriate Table. Throughout, $P < 0.05$ was taken as statistically significant
287 and where appropriate values of $P < 0.01$ and $P < 0.001$ are specified.

288

289

290

291 **Results**

292 **The novel CACHD1 protein is an $\alpha 2\delta$ paralog**

293 We first investigated the predicted protein domain structure of CACHD1. Figure 1A
 294 illustrates that, like $\alpha 2\delta$ -1, CACHD1 has a predicted exofacial N-terminus according to its
 295 signal sequence, a von Willebrand factor A (VWA) domain, two bacterial chemosensory-like
 296 cache domains and a short hydrophobic transmembrane domain followed by an intracellular
 297 C-terminus. Although CACHD1 and $\alpha 2\delta$ share limited amino acid sequence homology
 298 (<21%), the similarities in modular domain content and arrangement between the proteins
 299 suggested the possibility that CACHD1 represents an $\alpha 2\delta$ -like protein. However, there are
 300 also a number of differences between CACHD1 and $\alpha 2\delta$ -1; these include: (i) $\alpha 2\delta$ proteins
 301 are a single gene product which is post-translationally cleaved by proteases into $\alpha 2$ and
 302 δ components and then associate via disulphide bonding (Calderon-Rivera et al., 2012;
 303 Segura et al., 2017); an important 6 amino acid motif for proteolytic cleavage has been
 304 identified (Andrade et al., 2007) which is absent in CACHD1. (ii) CACHD1 has a single
 305 predicted post-translational N-glycosylation site, whilst $\alpha 2\delta$ -1 is heavily glycosylated at
 306 multiple potential sites (Douglas et al., 2006). (iii) CACHD1 has a variant RSR amino acid
 307 sequence at the binding site for gabapentinoids. (iv) Despite expressing a VWA domain, the
 308 functionally important MIDAS motif in CACHD1 (DxGxS) is different from that of $\alpha 2\delta$ -1
 309 (DxSxS). (v) $\alpha 2\delta$ s have a predicted GPI-anchoring site (Davies et al., 2010) which is absent
 310 in CACHD1, which instead has a predicted transmembrane domain and a larger intracellular
 311 C-terminus domain.

312 313 **CACHD1 is highly expressed in brain hippocampal and thalamic regions**

314 To obtain comparative and quantitative data on CACHD1 mRNA expression, real-time PCR
 315 was performed on rat and human mRNA from different regions of the brain and peripheral
 316 tissue. Relative expression profiles of CACHD1 and $\alpha 2\delta$ -1 transcripts in rat tissue showed
 317 high CACHD1 expression in thalamus, hippocampus and cerebellum, whilst $\alpha 2\delta$ -1 transcript
 318 expression was prominent in cortex, hippocampus and also, superior cervical ganglia (Fig.
 319 1B). We further investigated the anatomical distribution of CACHD1 at the transcriptional
 320 and protein levels using *in situ* hybridization and immunohistochemistry in adult mammalian
 321 brain. Rat brain regions displaying high mRNA include the hippocampus, anterodorsal
 322 thalamic nucleus, reticular thalamic nucleus, cerebellum, subiculum, medial entorhinal cortex
 323 and zona incerta (Fig. 1-1; Fig. 1-2). Hippocampal CACHD1 mRNA staining was strong in
 324 the dentate gyrus, as well as the CA1 pyramidal cell layer; mRNA staining was less strong in
 325 CA3. There was strong correlation between the levels of expression of CACHD1 mRNA and
 326 protein in rat brain (Fig. 1-2). In the thalamus, CACHD1 protein showed differential
 327 expression between major thalamic nuclei, in particular with prominent staining in the
 328 anterodorsal and reticular nuclei (Fig. 2). In human tissue, CACHD1 transcripts were
 329 similarly high in hippocampus, thalamus, and cerebellum (Fig. 2-1). CACHD1 transcript
 330 distribution was broadly similar to certain Cav3 subtypes, in particular to Cav3.1 (Fig. 2-1,
 331 Talley et al., 1999). CACHD1 transcript expression showed a differential distribution to $\alpha 2\delta$ -
 332 1 and $\alpha 2\delta$ -2 subtypes and was most similar to $\alpha 2\delta$ -3 (Fig. 2-1, Cole et al., 2005). In human
 333 tissue, CACHD1 protein levels were most abundant in dentate gyrus granule cells and
 334 pyramidal cells of the hippocampus cornu ammonis, cortical regions and thalamus, in both
 335 large diameter and small diameter cells (Fig. 3).

336

337 **CACHD1 promotes cell-surface expression of Cav3.1**

338 Our expression data indicated high levels of CACHD1 expression in the thalamus,
 339 hippocampus and cerebellum. As expression levels of Cav3 subunits are also high in the
 340 thalamus and hippocampus, we hypothesized that CACHD1 may modulate Cav3 subunits in
 341 a recombinant HEK cell system. As a first step, we expressed CACHD1 in HEK cells and
 342 confirmed the specificity of the CACHD1 antibody (Fig. 4A). Immunoreactive CACHD1 was
 343 detected at approximately 170 kDa. We also confirmed that CACHD1 is present at the cell-
 344 surface of HEK cells (Fig. 4B). Next, we determined if expression of CACHD1 affected the
 345 subcellular localization of Cav3.1 using a cell-surface biotinylation assay. Cell-surface
 346 proteins from HEK cells expressing empty vector, empty vector + CACHD1, GFP-Cav3.1-
 347 HA + empty vector and GFP-Cav3.1-HA + CACHD1 were extracted and levels of GFP-
 348 Cav3.1-HA analysed by Western blotting. Our data show that co-expression of CACHD1
 349 increased cell-surface localization of GFP-Cav3.1-HA (2.65 ± 0.40 fold over control $P < 0.05$
 350 two-tailed paired Student's *t*-test; Fig. 4C). We also quantified the whole-cell expression of
 351 GFP-Cav3.1-HA in the same HEK cells, normalising to levels to β -actin (Fig. 4D).
 352 Importantly, our data shows that CACHD1 increases levels of GFP-Cav3.1-HA at the cell-
 353 surface without affecting the total cellular level.

354 **CACHD1 and Cav3.1 are in close proximity at the cell-surface**

356 To determine if Cav3.1 and CACHD1 are present in a complex at the cell-surface, an epitope-
 357 tagged CACHD1 (Myc-CACHD1) was used to aid cell-surface precipitation and detection.
 358 First, we tested the expression of the tagged protein and examined the ability of an anti-Myc
 359 antibody to bind to CACHD1 at the cell-surface. Myc-CACHD1 was expressed in HEK cell
 360 with a similar molecular mass (~ 170 kDa) to untagged CACHD1 (Fig. 5-1). Furthermore, we
 361 could detect Myc-CACHD1 at the cell-surface using immunofluorescence and confocal

362 microscopy (Fig. 5-1). Proximity ligation assays are commonly used to predict the likelihood
 363 that two proteins are sufficiently close enough to be present in the same complex. First, we
 364 determined if we could simultaneously detect Myc-CACHD1 and GFP-Ca_v3.1-HA at the
 365 cell-surface by confocal microscopy. Live HEK cells expressing empty vector, empty vector
 366 + CACHD1, GFP-Ca_v3.1-HA + empty vector and GFP-Ca_v3.1-HA + CACHD1 were
 367 incubated with antibodies to the Myc and HA epitope tags of CACHD1 and Ca_v3.1,
 368 respectively and immunoreactive proteins visualized by immunofluorescence (Fig. 5A). No
 369 immunoreactive signals were detected in cells expressing empty vector, indicating antibody
 370 specificity. We were able to detect immunoreactive Myc signals only in cells expressing
 371 Myc-CACHD1. Similarly, we were able to detect signals for the HA antibody only in cells
 372 expressing GFP, indicating expression of GFP-Ca_v3.1-HA. We were also able to
 373 simultaneously detect CLR and RAMP1 at the cell-surface of transfected cells (Fig. 5A).
 374 Next, we labelled cells from the same transfections and performed a proximity ligation assay
 375 and visualized the cells using confocal microscopy. No PLA signals were detected in cells
 376 transfected with empty vector, empty vector + CACHD1, GFP-Ca_v3.1-HA + empty vector
 377 (Fig. 5B). By contrast, we could readily detect PLA signals in our positive control
 378 (CLR•RAMP1) and in transfected with GFP-Ca_v3.1-HA + CACHD1. Importantly, we could
 379 only detect PLA signals in cells expressing GFP (Fig. 5B). Thus, CACHD1 and Ca_v3.1 are in
 380 close proximity (<40 nm) at the cell-surface of HEK cells, indicating that they are likely in
 381 the same protein complex. As discussed more fully below, together, these data are consistent
 382 with CACHD1 increasing the cell-surface localization of Ca_v3.1 and with formation of
 383 CACHD1-Ca_v3.1 complexes at the cell surface.

384
 385 **CACHD1 modulates recombinant Ca_v3 family VGCCs**

386 We next tested the hypothesis that CACHD1 modulates T-type Ca^{2+} current. Co-expression
 387 of CACHD1 with $\text{Ca}_v3.1$ caused an increase in current density around peak values (Fig.
 388 6A,B) and a corresponding increase in maximal conductance (Fig. 6B inset; Table 1). By
 389 contrast, in our hands, $\text{Ca}_v3.1$ peak current and conductance was not modulated by $\alpha 2\delta-1$ in
 390 transfection-matched experiments (Fig. 6A,C; Table 1). CACHD1 effects were not
 391 accompanied by any overall change in the midpoint of activation or slope factor k (Table 1)
 392 and CACHD1 had no effect on $\text{Ca}_v3.1$ steady-state inactivation (data not shown). Neither
 393 CACHD1 nor $\alpha 2\delta-1$ affected $\text{Ca}_v3.1$ recovery from inactivation, as measured by lack of
 394 effect on mid-time of recovery from inactivation or τ_{recovery} ($p > 0.1$ for both, one-way
 395 ANOVA with Bonferroni post-hoc test, data not shown).

396 We next investigated potential modulation of $\text{Ca}_v3.2$ and $\text{Ca}_v3.3$ by CACHD1. Peak
 397 current density of $\text{Ca}_v3.2$ (Fig. 7A,C) and $\text{Ca}_v3.3$ (Fig. 7B,D) was increased by CACHD1
 398 with corresponding increases in maximal conductance (Table 1). CACHD1 had no significant
 399 effect on midpoint of activation or slope factor k for either $\text{Ca}_v3.2$ or $\text{Ca}_v3.3$ (Table 1) or
 400 steady-state inactivation ($p > 0.1$, Kruskal-Wallis test with Dunn's multiple comparison test,
 401 data not shown). CACHD1 was without effect on Ca_v3 activation or inactivation kinetics
 402 (Fig. 7-1; Table 1). In our hands, $\alpha 2\delta-1$ was without effect on current density in $\text{Ca}_v3.2$ (Fig.
 403 7E) or $\text{Ca}_v3.3$ (Fig. 7F). $\alpha 2\delta-1$ was without effect on $\text{Ca}_v3.2$ activation kinetics or on $\text{Ca}_v3.2$
 404 and $\text{Ca}_v3.3$ inactivation kinetics (Fig. 7-1; Table 1). $\alpha 2\delta-1$ had subtle effects on $\text{Ca}_v3.1$
 405 activation and inactivation kinetics and $\text{Ca}_v3.3$ activation kinetics (Fig. 7-1; Table 1).
 406 Overall, these data suggest that CACHD1, but not $\alpha 2\delta-1$, has a major effect on recombinant
 407 Ca_v3 VGCCs in terms of increased Ca^{2+} current density and maximal conductance.

408 To determine the mechanism by which CACHD1 increased T-type channel currents,
 409 we estimated channel opening probability by measuring $\text{Ca}_v3.1$ gating currents at the reversal

410 potential for the ionic current (Fig. 8). In these experiments, the CACHD1-mediated increase
 411 in current density was recapitulated; thus, $\text{Ca}_v3.1$ maximal conductance 280 ± 30 pS/pF was
 412 significantly increased to 860 ± 15 pA/pF ($n = 12$ for each condition from 3 separate
 413 transfections; $P < 0.001$ Mann-Whitney test) (data not shown). Measurement of area under the
 414 gating current provides a measure of the maximal gating charge Q_{max} . A plot of conductance
 415 versus gating current amplitude of the ionic current of the same cell provides a measure of
 416 open probability (P_o) (Agler et al., 2005). Under these conditions, there was a ~ 1.4 fold
 417 increase in $\text{Ca}_v3.1$ P_o in CACHD1 expressing cells ($P < 0.001$, Fig. 8). These findings are
 418 consistent with CACHD1 interaction with $\text{Ca}_v3.1$ at the cell surface causing a functional
 419 increase in P_o as a major contribution to CACHD1-mediated increases in Ca^{2+} current
 420 density.

423 **CACHD1 increase Ca_v3 -mediated excitability in hippocampal neurons**

424 Ca_v3 channels are predicted to affect neuronal excitability around the resting membrane
 425 potential (Perez-Reyes, 2003; Cheong and Shin, 2013). To investigate the role of CACHD1
 426 in controlling neuronal excitability, we expressed CACHD1 (vs. empty vector controls) in
 427 hippocampal neurons. Transfected neurons were identified by co-expression of the biomarker
 428 mVenus (Fig. 9A). At a depolarizing current injection step of 220 pA, CACHD1 expressing
 429 neurons fired at a higher frequency than control neurons (Fig. 9B,C,D; Table 2). To further
 430 determine the role of T-type currents in establishing the increase in neuronal firing
 431 frequencies, we used the selective Ca_v3 channel blocker, TTA-P2 (Dreyfus et al., 2010).
 432 TTA-P2 (1 μM) reversed the firing frequency in CACHD1 expressing neurons back to
 433 control levels, but was without effect on control neurons (Fig. 9D; Table 2). To increase the

434 contribution of T-type current to neuronal excitability, a hyperpolarizing prepulse was used to
435 recover LVA Ca^{2+} channels from inactivation, followed by a short depolarizing pulse to
436 evoke an AP (Eckle et al., 2014). Under these conditions, CACHD1 expression caused a
437 more profound increase in rebound firing frequency in CACHD1-transfected, but not control,
438 neurons (Fig. 9E,F,G; Table 2). TTA-P2 (1 μM) reversed the increase in rebound AP firing
439 in CACHD1 expressing neurons back to control levels, but was without effect on control
440 neurons (Fig. 9G; Table 2). Throughout these experiments, CACHD1 had no significant
441 effects on AP waveform properties (Fig. 9-1). These data support a CACHD1-mediated
442 selective increase in T-type Ca^{2+} current, which leads to an increase in AP firing frequency
443 and excitability in native neurons.

444 **Discussion**

445 This study characterises the protein CACHD1, encoded by the cache domain containing 1
 446 gene, and presents evidence that it represents a novel protein that modulates Ca_v3 VGCC
 447 activity. These data also provide further evidence that the major α 2 δ -1 auxiliary calcium
 448 channel subunit does not fulfil a similar role for Ca_v3 channels. Detailed examination of
 449 Ca_v3.1 channels suggests an underlying mechanism whereby CACHD1 promotes increased
 450 Ca_v3.1 levels at the plasma membrane. In addition, data were consistent with CACHD1
 451 forming a complex with the channel at the cell surface to increase open probability and
 452 potentiate T-type current.

453

454 **CACHD1 protein modulates Ca_v3 VGCCs**

455 At a cellular level, CACHD1 transcripts were localised to granule and pyramidal cells of the
 456 hippocampus, and specific thalamic nuclei, notably the anterodorsal thalamic nucleus and
 457 reticular nucleus. Compared to the gene expression of the major α 2 δ -1 and α 2 δ -2 subunits,
 458 CACHD1 protein displayed a unique expression signature with, in particular, high expression
 459 in the thalamus and hippocampus and also in some regions of the cerebellum and cortex.
 460 CACHD1 was largely co-incident with the expression pattern of the Ca_v3.1 channel in the
 461 CNS (Talley et al., 1999). CACHD1 co-transfection with Ca_v3.1 in recombinant cells
 462 increased cell surface expression and Ca²⁺ current levels and maximal conductance.
 463 CACHD1 similarly modulated Ca_v3.2 and Ca_v3.3 current levels. Under equivalent
 464 conditions, α 2 δ -1 was without significant effect on current levels in any Ca_v3 subtype.
 465 Proximity ligation assays were consistent with CACHD1 being able to form complexes with
 466 Ca_v3.1 at the cell surface. Mechanistically, CACHD1 effects on Ca_v3.1 were associated with
 467 increases in channel Po. A similar role has been reported for α 2 δ auxiliary subunit

interactions with Ca_v1 channels; thus, $\alpha 2\delta$ -1 increased channel Po and channel number as well as allosterically regulating drug binding (Shistik et al., 1995; Wei et al., 1995). Other studies have reported either an $\alpha 2\delta$ -mediated reduction in Po (Wakamori et al., 1999) or a lack of effect on Po (Brodbeck et al., 2002). The latter study suggested that $\alpha 2\delta$ predominantly performs a VGCC trafficking function to increase the number of active channels at the membrane (reviewed by Dolphin, 2012). The demonstrated CACHD1-mediated increase in $\text{Ca}_v3.1$ cell surface expression is proposed to contribute to increase in cell Ca^{2+} current levels and maximal conductance. Here, the ~ 1.4 -fold increase in Po is insufficient to fully account for the ~ 3 fold increase in current density seen in this set of experiments; channel number is predicted to increase (according to $I = iN\text{Po}$, where I is the whole-cell current, i is the single channel current (predicted to be constant) and N is the number of functional channels). Thus, increase in channel number may be attributable to either CACHD1-mediated increases in forward trafficking or reduced endocytosis of $\text{Ca}_v3.1$. With respect to $\alpha 2\delta$ auxiliary subunits, HVA $\text{Ca}_v\alpha 1$ - $\alpha 2\delta$ interactions are reported to occur during early maturation at an intracellular site to drive forward trafficking to the plasma membrane (Cantí et al., 2005). Whilst $\text{Ca}_v2.2$ proteomic data have reported only a low appreciable amount of co-purified $\alpha 2\delta$, with detection dependent on solubilising agent used (Müller et al., 2010), recent work using exofacial tags and antigen stripping techniques has supported $\alpha 2\delta$ also remaining associated with $\text{Ca}_v2.2$ at the plasma membrane (Cassidy et al., 2014). In the present study, clear indication of CACHD1 and $\text{Ca}_v3.1$ complex formation at the cell surface was obtained using proximity ligand assays. Moreover, $\alpha 2\delta$ has the propensity to sequester into lipid raft compartments, as reported by us (Ronzitti et al., 2015) and others; this may also limit efficient detection of $\alpha 2\delta$ - $\text{Ca}_v\alpha 1$ complexes and it will be of interest to determine if CACHD1 similarly localizes to lipid rafts. Overall, we propose that

492 CACHD1 acts to increase Cav3 expression at the plasma membrane, at the cell surface
 493 CACHD1 can form a complex with the channel to increase Po and, consequentially, increase
 494 T-type current.

495

496 **Potential functional impact of CACHD1 on Cav3 VGCCs**

497 T-type Ca^{2+} currents are active around the resting membrane potential, where non-
 498 inactivating channels generate low threshold Ca^{2+} spikes and the consequential triggering of
 499 Na^{+} -dependant APs (Llinás 1988; Cheong and Shin, 2013). Of further interest here is that
 500 multiple mechanisms and proteins involved in folding and trafficking are reported to be
 501 involved in Cav3 expression at the cell surface. For example, proteins such the actin binding
 502 protein kelch-like 1 (Aromomolaran et al., 2010), stac1 (Rzhpetskyy et al., 2016) and
 503 calnexin (Proft et al., 2017) have a proposed role in Cav3 expression. Moreover, the
 504 glycosylated form of Cav3 represents the mature, correctly folded protein that is associated
 505 with higher Po (Weiss et al., 2013; Ondacova et al., 2016). T-type current has also been
 506 implicated in regulating presynaptic transmitter release in hippocampal and nociceptive
 507 circuitry (Huang et al., 2011; Jacus et al., 2012). Increases in Cav3 current are predicted to
 508 have profound effects on neuronal firing (McCormick and Huguenard, 1992).
 509 Correspondingly, over-expression of CACHD1 caused a pronounced increase in T-type
 510 current-mediated spike firing in hippocampal neurons. This activity was enhanced using a
 511 protocol to trigger recovery of Cav3 channels from their inactivated states, thereby increasing
 512 contribution of T-type current to neuronal excitability. Cav3 subtypes have been suggested as
 513 targets for anti-epileptic drugs (Powell et al., 2014). In models of temporal lobe epilepsy
 514 (TLE), selective up-regulation of T-type current in hippocampal neurons causes intrinsic
 515 bursting activity (Sanabria et al., 2001; Su et al., 2002). Cav3.2 transcripts were upregulated

516 in TLE models and intrinsic burst firing was reduced in $\text{Ca}_v3.2$ knock-out mice (Becker et
 517 al., 2008). Moreover, the deubiquitinating enzyme USP5 (Garcia-Callero et al., 2014), and
 518 preventing $\text{Ca}_v3.2$ deubiquitination was suggested to be beneficial in neuropathic and
 519 inflammatory pain. Our data suggest CACHD1 as a potential future target in
 520 hyperexcitability disorders associated with Ca_v3 dysfunction, such as epilepsy and pain.
 521 Moreover, CACHD1 gene expression has been shown to be modulated in patients with Type
 522 1 diabetes (Rassi et al., 2008) and Parkinson's disease (Aguilar and Severino, 2010).

523

524 **CACHD1 protein structure dictates $\alpha 2\delta$ -like function**

525 There are clear similarities in protein structural motifs between CACHD1 and $\alpha 2\delta$, namely,
 526 the presence of an N-terminal signal sequence, VWA and two downstream cache domains,
 527 these similarities suggest a conserved evolution (Anantharaman and Aravind, 2000).
 528 However, a number of important differences are also present. CACHD1 has a RSR variant at
 529 the gabapentin binding motif; whilst $\alpha 2\delta$ -1 and $\alpha 2\delta$ -2 were found to bind to gabapentinoids
 530 via their RRR binding motif, $\alpha 2\delta$ -3 and $\alpha 2\delta$ -4 have variant RNR sites which do not bind
 531 gabapentin (Wang et al., 1999; Marais et al., 2001). Earlier studies also identified porcine
 532 $\alpha 2\delta$ -1 residues 516 to 537 within the first cache domain and residues 583 to 603 as also
 533 contributing to gabapentin binding (Wang et al., 1999). It will be of interest to determine if
 534 CACHD1 binds gabapentinoids. Despite sharing a common VWA domain, CACHD1 has a
 535 variant MIDAS motif. The $\alpha 2\delta$ -1 MIDAS motif is functionally important in Ca^{2+} channel
 536 trafficking and synaptic function (Canti et al., 2005; Hoppa et al., 2012). However, it has
 537 been suggested that MIDAS is unlikely to represent a key $\text{Ca}_v2.2/\alpha 2\delta$ -1 interaction site,
 538 rather other regions are more likely involved (Cassidy et al., 2014); such regions may include
 539 cache domains, for example, rat $\alpha 2\delta$ -1 residues 751-755, which are within a modelled cache

540 region, were implicated in $\text{Ca}_v2.2/\alpha2\delta$ -1 interaction (Cassidy et al., 2014). By contrast,
 541 comparative data investigating $\alpha2\delta$ effects on $\text{Ca}_v1.2$ point to aspartate and the first serine
 542 residue within the DxSxS MIDAS site as molecular determinants for interaction and correct
 543 modulation of $\text{Ca}_v1.2$ (Briot et al., 2018). Of interest here is that CACHD1 contains a variant
 544 MIDAS with a glycine residue at the equivalent position of the critical serine residue
 545 identified by Briot et al. (2018). It has also been proposed that the $\alpha2\delta$ amino terminal
 546 (amino acids 26-230, termed the R-domain) contains all the machinery required to support
 547 $\alpha2\delta$ -1-mediated current enhancement in $\text{Ca}_v2.2$ channels (Song et al., 2015). This study
 548 identified a tryptophan residue (W205), which is conserved across all four $\alpha2\delta$ isoforms, as
 549 an important molecular determinant for these R-domain effects; it is of note that CACHD1
 550 also contains a conserved tryptophan residue at the equivalent position.

551 In bacteria, the cache domain is proposed to arise from bacterial small molecule
 552 binding domains PAS and GAF (Anantharaman et al., 2001) and to play a key role in
 553 chemotaxis by acting as an extracellular receptor (Anantharaman and Aravind, 2000). Recent
 554 computational work has suggested that cache domains represent the dominant extracellular
 555 sensor in prokaryotes; by contrast, cache domains are largely limited to only $\alpha2\delta$ subunits in
 556 metazoa (Upadhyay et al., 2016). The present study adds CACHD1 to this classification.
 557 Whilst the functional relevance of mammalian cache domains remains to be fully established,
 558 deletions within the cache domain of $\alpha2\delta$ -4 have been associated with familial bipolar
 559 disorder (Van Den Bossche et al., 2010). Roles for ‘free’ $\alpha2\delta$ (not associated with VGCCs)
 560 have also been extended to functions including synaptogenesis and neurodegeneration via
 561 interaction with alternative ligands such as thrombospondins and prion proteins, respectively
 562 (Eroglu et al., 2009, Lana *et al.*, 2016; Senatore et al., 2012); it will also be of interest to see
 563 if CACHD1 possesses similar functionality.

564 Overall, our data are consistent with CACHD1 structurally representing an $\alpha 2\delta$ -like
565 protein that act to increase Ca_v3 cell surface expression and current. Identification of the
566 CACHD1 protein as a modulator of Ca_v3 activity expands the range of VGCC associated
567 proteins and may provide an additional target itself, or via its modulation of T-type current, in
568 different disease states.
569

570 **References**

571 Agler HL, Evans J, Tay LH, Anderson MJ, Colecraft HM, Yue DT (2005) G protein-gated
572 inhibitory module of N-type (Cav2.2) Ca²⁺ channels. *Neuron* 46:891-904.

573

574 Aguiar PM, Severino P (2010) Biomarkers in Parkinson Disease: global gene expression
575 analysis in peripheral blood from patients with and without mutations in PARK2 and
576 PARK8. *Einstein (Sao Paulo)* 8:291-297.

577

578 Anantharaman V, Aravind L (2000) Cache - a signaling domain common to animal Ca²⁺-
579 channel subunits and a class of prokaryotic chemotaxis receptors. *Trends Biochem Sci*
580 25:535-537.

581

582 Anantharaman V, Koonin EV, Aravind L (2001) Regulatory potential, phyletic distribution
583 and evolution of ancient, intracellular small-molecule-binding domains. *J Mol Biol* 307:
584 1271-1292.

585

586 Andrade A, Sandoval A, Oviedo N, De Waard M, Elias D, Felix R (2007) Proteolytic
587 cleavage of the voltage-gated Ca²⁺ channel $\alpha 2\delta$ subunit: structural and functional features.
588 *Eur J Neurosci* 25:1705-1710.

589

590 Aromolaran KA, Benzow KA, Cribbs LL, Koob MD, Piedras-Rentería ES (2010) T-type
591 current modulation by the actin-binding protein Kelch-like 1. *Am J Physiol Cell*
592 *Physiol* 298:C1353–1362.

593

594

595 Baumgart JP, Vitko I, Bidaud I, Kondratskyi A, Lory P, Perez-Reyes E (2008) I-II loop
 596 structural determinants in the gating and surface expression of low voltage-activated calcium
 597 channels. PLoS ONE 3:e2976.

598

599 Becker AJ, Pitsch J, Sochivko D, Opitz T, Staniek M, Chen CC, Campbell KP, Schoch S,
 600 Yaari Y, Beck H (2008) Transcriptional upregulation of Cav3.2 mediates epileptogenesis in
 601 the pilocarpine model of epilepsy. J Neurosci 28:13341-13353.

602

603 Briot J, Mailhot O, Bourdin B, Tétreault MP, Najmanovich R, Parent L (2018) A three-way
 604 inter-molecular network accounts for the Cav α 2 δ 1-induced functional modulation of the
 605 pore-forming Cav1.2 subunit. J Biol Chem Mar 27 [Epub ahead of print].

606

607 Brodbeck J, Davies A, Courtney JM, Meir A, Balaguero N, Cantí C, Moss FJ, Page KM,
 608 Pratt WS, Hunt SP, Barclay J, Rees M, Dolphin AC (2002) The ducky mutation in Cacna2d2
 609 results in altered Purkinje cell morphology and is associated with the expression of a
 610 truncated α 2 δ 2 protein with abnormal function. J Biol Chem 277:7684-7693.

611

612 Calderon-Rivera A, Andrade A, Hernández-Hernández O, González-Ramírez R, Sandoval A,
 613 Rivera M, Gomora JC, Felix R (2012) Identification of a disulfide bridge essential for
 614 structure and function of the voltage-gated Ca²⁺ channel α 2 δ -1 auxiliary subunit. Cell
 615 Calcium 51:22–30.

616

- 617 Cantí C, Nieto-Rostro M, Foucault I, Heblich F, Wratten J, Richards MW, Hendrich J,
 618 Douglas L, Page KM, Davies A, Dolphin AC (2005) The metal-ion-dependent adhesion site
 619 in the Von Willebrand factor-A domain of $\alpha 2\delta$ subunits is key to trafficking voltage-gated
 620 Ca^{2+} channels. *Proc Natl Acad Sci U S A* 102:11230-11235.
- 621
- 622 Cassidy JS, Ferron L, Kadurin I, Pratt WS, Dolphin AC (2014) Functional exofacially tagged
 623 N-type calcium channels elucidate the interaction with auxiliary $\alpha 2\delta$ -1 subunits. *Proc Natl*
 624 *Acad Sci U S A* 111: 8979-8984.
- 625
- 626 Cheong E, Shin HS (2013) T-type Ca^{2+} channels in normal and abnormal brain functions.
 627 *Physiol Rev* 93:961-992.
- 628
- 629 Cole R, Lechner SM, Williams ME, Prodanovich P, Bleicher L, Varney MA, Gu G (2005)
 630 Differential distribution of voltage-gated calcium channel alpha-2 delta ($\alpha 2\delta$) subunit
 631 mRNA-containing cells in the rat central nervous system and the dorsal root ganglia. *J Comp*
 632 *Neurol* 491:246-269.
- 633
- 634 Cottrell GS, Padilla B, Pikios S, Roosterman D, Steinhoff M, Grady EF, Bunnett NW (2007)
 635 Post-endocytic sorting of calcitonin receptor-like receptor and receptor activity-modifying
 636 protein 1. *J Biol Chem* 282:12260-12271.
- 637
- 638 Davies A, Kadurin I, Alvarez-Laviada A, Douglas L, Nieto-Rostro M, Bauer CS, Pratt WS,
 639 Dolphin AC (2010) The $\alpha 2\delta$ subunits of voltage-gated calcium channels form GPI anchored

640 proteins, a posttranslational modification essential for function. *Proc Natl Acad Sci U S A*
 641 107:1654–1659.
 642
 643 Dolphin AC, Wyatt CN, Richards J, Beattie RE, Craig P, Lee JH, Cribbs LL, Volsen SG,
 644 Perez-Reyes E (1999) The effect of $\alpha 2\delta$ and other accessory subunits on expression and
 645 properties of the calcium channel $\alpha 1G$. *J Physiol* 519:35-45.
 646
 647 Dolphin AC (2012) Calcium channel auxiliary $\alpha 2\delta$ and β subunits: trafficking and one step
 648 beyond. *Nat Rev Neurosci* 13:542-555.
 649
 650 Dolphin AC (2013) The $\alpha 2\delta$ subunits of voltage-gated calcium channels. *Biochim Biophys*
 651 *Acta* 1828:541-1549.
 652
 653 Dooley DJ, Taylor CP, Donevan S, Feltner D (2007) Ca^{2+} channel $\alpha 2\delta$ ligands: novel
 654 modulators of neurotransmission. *Trends Pharmacol Sci* 28:75-82.
 655
 656 Douglas L, Davies A, Wratten J, Dolphin AC (2006) Do voltage-gated calcium channel $\alpha 2\delta$
 657 subunits require proteolytic processing into $\alpha 2$ and δ to be functional? *Biochem Soc Trans*
 658 34:894-898.
 659
 660 Dreyfus FM, Tscherter A, Errington AC, Renger JJ, Shin HS, Uebele VN, Crunelli V,
 661 Lambert RC, Leresche N (2010) Selective T-type calcium channel block in thalamic neurons
 662 reveals channel redundancy and physiological impact of $I_{Twindow}$. *J Neurosci* 30:99-109.
 663

664 Dubel S, Altier C, Chaumont S, Lory P, Bourinet E, Nargeot J (2004) Plasma membrane
 665 expression of T-type calcium channel $\alpha 1$ subunits is modulated by high voltage-activated
 666 auxiliary subunits. *J Biol Chem* 279:29263-29269.
 667
 668 Eckle V-S, Shcheglovitov A, Vitko I, Dey D, Yap CC, Winckler B, Perez-Reyes E (2014)
 669 Mechanisms by which a *CACNA1H* mutation found in epilepsy patients increases seizure
 670 susceptibility. *J Physiol* 592:795-809.
 671
 672 Eroglu C, Allen NJ, Susman MW, O'Rourke NA, Park CY, Ozkan E, Chakraborty C,
 673 Mulinyawe SB, Annis DS, Huberman AD, Green EM, Lawler J, Dolmetsch R, Garcia KC,
 674 Smith SJ, Luo ZD, Rosenthal A, Mosher DF, Barres BA (2009) Gabapentin receptor $\alpha 2\delta$ -1 is
 675 a neuronal thrombospondin receptor responsible for excitatory CNS synaptogenesis. *Cell*
 676 139:380-392.
 677
 678 García-Caballero A, Gadotti VM, Stemkowski P, Weiss N, Souza IA, Hodgkinson V, Bladen
 679 C, Chen L, Hamid J, Pizzoccaro A, Deage M, François A, Bourinet E, Zamponi GW (2014)
 680 The deubiquitinating enzyme USP5 modulates neuropathic and inflammatory pain by
 681 enhancing Cav3.2 channel activity. *Neuron* 83:1144-1158.
 682
 683 Hoppa M, Lana B, Margas W, Dolphin AC, Ryan TA (2012) $\alpha 2\delta$ couples calcium channels
 684 to neurotransmitter release sites to control release probability. *Nature* 486:122-125.
 685

686 Huang Z, Lujan R, Kadurin I, Uebele VN, Renger JJ, Dolphin AC, Shah MM (2011)
 687 Presynaptic HCN1 channels regulate $\text{Ca}_v3.2$ activity and neurotransmission at select cortical
 688 synapses. *Nat Neurosci* 14:478-486.
 689
 690 Jacus MO, Uebele VN, Renger JJ, Todorovic SM (2012) Presynaptic $\text{Cav}3.2$ channels
 691 regulate excitatory neurotransmission in nociceptive dorsal horn neurons. *J Neurosci* 32:
 692 9374-9382.
 693
 694 Jones PJ, Wang Y, Smith MD, Hargus NJ, Eidam HS, White HS, Kapur J, Brown ML, Patel
 695 MK (2007) Hydroxyamide analogs of propofol exhibit state-dependent block of sodium
 696 channels in hippocampal neurons: implications for anticonvulsant activity *J Pharmacol Exp*
 697 *Ther* 320:828-36.
 698
 699 Lacinová L, Klugbauer N, Hofmann F (1999) Absence of modulation of the expressed
 700 calcium channel $\alpha_1\text{G}$ subunit by $\alpha_2\delta$ subunits. *J Physiol* 516:639-645.
 701
 702 Lana B, Page KM, Kadurin I, Ho S, Nieto-Rostro M, Dolphin AC (2016) Thrombospondin-4
 703 reduces binding affinity of [^3H]-gabapentin to calcium-channel $\alpha_2\delta$ -1 subunit but does not
 704 interact with $\alpha_2\delta$ -1 on the cell-surface when co-expressed. *Sci Rep* 6:24531
 705
 706 Llinás RR (1988) The intrinsic electrophysiological properties of mammalian neurons:
 707 insights into central nervous system function. *Science* 242:1654-1664.
 708

709 Marais E, Klugbauer N, Hofmann F (2001) Calcium channel $\alpha 2\delta$ subunits-structure and
 710 gabapentin binding. *Mol Pharmacol* 59:1243-1248.
 711

712 McCormick DA, Huguenard JR (1992) A model of the electrophysiological properties of
 713 thalamocortical relay neurons. *J Neurophysiol* 68:1384-1400.
 714

715 Müller CS, Haupt A, Bildl W, Schindler J, Knaus HG, Meissner M, Rammner B, Striessnig J,
 716 Flockerzi V, Fakler B, Schulte U (2010) Quantitative proteomics of the Cav2 channel nano-
 717 environments in the mammalian brain. *Proc Natl Acad Sci U S A* 107:14950-14957.
 718

719 Ondacova K, Karmazinova M, Lazniewska J, Weiss N, Lacinova L (2016) Modulation of
 720 Cav3.2 T-type calcium channel permeability by asparagine-linked glycosylation. *Channels*
 721 (Austin) 10:175–184.
 722

723 Perez-Reyes E (2003) Molecular physiology of low-voltage-activated T-type calcium channels.
 724 *Physiol Rev* 83:117-161.
 725

726 Powell KL, Cain SM, Snutch TP, O'Brien TJ (2014) Low threshold T-type calcium channels
 727 as targets for novel epilepsy treatments. *Br J Clin Pharmacol* 77:729-739.
 728

729 Proft J, Rzhetsky Y, Lazniewska J, Zhang FX, Cain SM, Snutch TP, Zamponi G, Weiss
 730 N (2017) The Cacna1h mutation in the GAERS model of absence epilepsy enhances T-type
 731 Ca^{2+} currents by altering calnexin-dependent trafficking of Cav3.2 channels. *Sci Rep*
 732 7:11513.

733

734 Rassi DM, Junta CM, Fachin AL, Sandrin-Garcia P, Mello S, Silva GL, Evangelista AF,
 735 Magalhães DA, Wastowski IJ, Crispim JO, Martelli-Palomino G, Fernandes AP, Deghaide
 736 NN, Foss-Freitas MC, Foss MC, Soares CP, Sakamoto-Hojo ET, Passos GA, Donadi EA
 737 (2008) Gene expression profiles stratified according to type 1 diabetes mellitus susceptibility
 738 regions. *Ann N Y Acad Sci* 1150:282-289.

739

740 Ronzitti G, Bucci G, Emanuele M, Leo D, Sotnikova TD, Mus LV, Soubrane CH, Dallas
 741 ML, Thalhammer A, Cingolani LA, Mochida S, Gainetdinov RR, Stephens GJ, Chieregatti E
 742 (2014) Exogenous α -synuclein decreases raft partitioning of Cav2.2 channels inducing
 743 dopamine release. *J Neurosci* 34:10603-10615.

744

745 Rzhepetsky Y, Lazniewska J, Proft J, Campiglio M, Flucher BE, Weiss N (2016) A
 746 Cav3.2/Stac1 molecular complex controls T-type channel expression at the plasma
 747 membrane. *Channels (Austin)* 10:346–354.

748

749 Sanabria ER, Su H, Yaari Y (2001) Initiation of network bursts by Ca^{2+} -dependent intrinsic
 750 bursting in the rat pilocarpine model of temporal lobe epilepsy. *J Physiol* 532:205-216.

751

752 Schneider R, Hosy E, Kohl J, Klueva J, Choquet D, Thomas U, Voigt A, Heine M (2015)
 753 Mobility of calcium channels in the presynaptic membrane. *Neuron* 86:672-679.

754

755 Segura E, Bourdin B, Tétreault MP, Briot J, Allen BG, Mayer G, Parent L (2017) Proteolytic
 756 cleavage of the hydrophobic domain in the $\text{Ca}_v\alpha 2\delta 1$ subunit improves assembly and activity
 757 of cardiac $\text{Ca}_v1.2$ channels. *J Biol Chem* 292:11109-11124.
 758
 759 Senatore A, Colleoni S, Verderio C, Restelli E, Morini R, Condliffe SB, Bertani I, Mantovani
 760 S, Canovi M, Micotti E, Forloni G, Dolphin AC, Matteoli M, Gobbi M, Chiesa R (2012)
 761 Mutant PrP suppresses glutamatergic neurotransmission in cerebellar granule neurons by
 762 impairing membrane delivery of VGCC $\alpha 2\delta$ -1 subunit. *Neuron* 74:300-313.
 763
 764 Shcheglovitov A, Vitko I, Bidaud I, Baumgart JP, Navarro-Gonzalez MF, Grayson TH, Lory
 765 P, Hill CE, Perez-Reyes E (2008) Alternative splicing within the I-II loop controls surface
 766 expression of T-type $\text{Ca}_v3.1$ calcium channels. *FEBS Lett* 582, 3765–3770.
 767
 768 Shistik E, Ivanina T, Puri T, Hosey M, Dascal N (1995) Ca^{2+} current enhancement by $\alpha 2/\delta$
 769 and β subunits in *Xenopus* oocytes: contribution of changes in channel gating and $\alpha 1$ protein
 770 level. *J Physiol* 489:55-62.
 771
 772 Snutch TP, Zamponi GW (2017) Recent advances in the development of T-type calcium
 773 channel blockers for pain intervention. *Br J Pharmacol* Jun 13 [Epub ahead of print].
 774
 775 Song L, Espinoza-Fuenzalida IA, Etheridge S, Jones OT, Fitzgerald EM (2015) The R-
 776 domain: Identification of an N-terminal region of the $\alpha 2\delta$ -1 subunit which is necessary and
 777 sufficient for its effects on $\text{Ca}_v2.2$ calcium currents. *Curr Mol Pharmacol* 8:169-179.
 778

779
 780 Soubrane CH, Stevens EB, Stephens GJ (2012) Expression and functional studies of the
 781 novel CNS protein CACHD1. Physiology 2012 (Edinburgh) Proc Physiol Soc 27, PC74.
 782
 783 Su H, Sochivko D, Becker A, Chen J, Jiang Y, Yaari Y, Beck H (2002) Upregulation of a T-
 784 type Ca^{2+} channel causes a long-lasting modification of neuronal firing mode after status
 785 epilepticus. J Neurosci 22:3645-3655.
 786
 787 Talley E, Cribbs LL, Lee JH, Daud A, Perez-Reyes E, Bayliss DA (1999) Differential
 788 distribution of three members of a gene family encoding low voltage-activated (T-type)
 789 calcium channels. J Neurosci 19:1895-1911.
 790
 791 Upadhyay AA, Fleetwood AD, Adebali O, Finn RD, IB ZN (2016) Cache domains that are
 792 homologous to, but different from PAS domains comprise the largest superfamily of
 793 extracellular sensors in prokaryotes. PLoS Comput Biol 12:e1004862.
 794
 795 Van Den Bossche MJ, Strazisar M, De Bruyne S, Bervoets C, Lenaerts AS, De Zutter S,
 796 Nordin A, Norrback KF, Goossens D, De Rijk P, Green EK, Grozeva D, Mendlewicz J,
 797 Craddock N, Sabbe BG, Adolfsson R, Souery D, Del-Favero J (2012) Identification of a
 798 CACNA2D4 deletion in late onset bipolar disorder patients and implications for the
 799 involvement of voltage-dependent calcium channels in psychiatric disorders. Am J Med
 800 Genet B Neuropsychiatr Genet 159B:465-475.
 801

802 Vogl C, Tanifuji S, Danis B, Daniels V, Foerch P, Wolff C, Whalley BJ, Mochida S,
803 Stephens GJ (2015) Synaptic vesicle glycoprotein 2A modulates vesicular release and
804 calcium channel function at peripheral sympathetic synapses. *Eur J Neurosci* 41:398-409.
805
806 Wakamori M, Mikala G, Mori Y (1999) Auxiliary subunits operate as a molecular switch in
807 determining gating behaviour of the unitary N-type Ca^{2+} channel current in *Xenopus* oocytes.
808 *J Physiol* 517:659-72.
809
810 Wang M, Offord J, Oxender D, Su T (1999) Structural requirement of the calcium-channel
811 subunit $\alpha 2\delta$ for gabapentin binding. *Biochem J* 342:313-320.
812
813 Wei X, Pan S, Lang W, Kim H, Schneider T, Perez-Reyes E, Birnbaumer L (1995) Molecular
814 determinants of cardiac Ca^{2+} channel pharmacology. Subunit requirement for the high affinity
815 and allosteric regulation of dihydropyridine binding. *J Biol Chem* 270:27106-27111.
816
817 Weiss N, Black SA, Bladen C, Chen L, Zamponi GW (2013) Surface expression and function
818 of Cav3.2 T-type calcium channels are controlled by asparagine-linked glycosylation.
819 *Pflugers Arch* 465:1159-1170.
820
821 Zhang H, Webb DJ, Asmussen H, Horwitz AF (2003) Synapse formation is regulated by the
822 signaling adaptor GIT1. *J Cell Biol* 161:131-142.
823
824

825 **Figure Legends**

826 **Figure 1. Predicted protein sequence homology and relative expression profile of**

827 **CACHD1 and $\alpha 2\delta$ -1.**

828 CACHD1 and $\alpha 2\delta$ -1 subunits both contain a N-terminus signal peptide, a VWA domain, two

829 cache domains, and transmembrane and intracellular domains. GBP: gabapentin binding

830 domain (RRR). GBP*: gabapentin binding domain variant (RSR). MIDAS: metal-ion-

831 dependent adhesion site (DxSxS). MIDAS*: metal-ion-dependent adhesion site variant

832 (DxGxS). VWA: von Willebrand factor A. Cache: Ca^{2+} channel and chemotaxis receptor.

833 TM: transmembrane domain. Cys: cysteine. His: histidine (locations of domains are

834 approximate and from data from www.Uniprot.org, figure drawn using DOG: Domain

835 Graphics). (B) Relative expression profile of CACHD1 and $\alpha 2\delta$ -1 mRNA in rat tissue

836 determined using SYBR green real-time quantitative PCR and HPRT1 as housekeeping gene.

837 DRG: dorsal root ganglion. SCG: superior cervical ganglion. (Data normalised to lowest

838 tissue expression; n=3 experiments using 3 animals each). Figure 1 is supported by *in situ*

839 hybridization data in different rat brain regions (Fig. 1-1) and qualitative expression profile of

840 CACHD1 mRNA and protein in the adult rat brain (Fig. 1-2).

841

842 **Figure 2. CACHD1 protein expression in adult rat brain.**

843 Immunoreactive protein was detected using rabbit anti-CACHD1 with peroxidase anti-rabbit

844 secondary antibody and DAB staining (brown). AD: anterodorsal thalamic nucleus; AVDM:

845 anteroventral thalamic nucleus (dorsomedial); AVVL: anteroventral thalamic nucleus

846 (ventro-lateral); fi: fimbria; MD: mediodorsal thalamic nucleus; Po: posterior thalamic

847 nucleus; sm: strai medullaris; Rt: reticular thalamus nucleus; RtSt: reticular VL: ventrolateral

848 thalamic nucleus; VPL: ventro-posterior lateral thalamus; g: granule cell layer; m: molecular

layer; p: Purkinje cell; wm: white matter. Figure 2 is supported by expression profiling of CACHD1 and different voltage-gated calcium channel subunit mRNA in human tissue (Fig. 2-1).

Figure 3. CACHD1 protein expression in human brain.

Immunohistochemistry of adult human brain using rabbit anti-CACHD1 with peroxidase anti-rabbit secondary antibody with (brown) DAB stain. CA1-3: cornus ammonis 1-3; DG: dentate gyrus.

Figure 4. Characterisation of CACHD1 and its effects on Cav3.1 channel expression.

HEK cells were transfected with empty vector (vector control, VC), CACHD1, Myc-CACHD1, GFP-Cav3.1-HA alone or in combination, as shown in each panel. (A) HEK cell lysates were analysed by Western blotting (WB). An antibody to CACHD1 recognised a single protein similar to the predicted size for CACHD1, but also recognized a non-specific protein in all lysates. (B) Cell-surface proteins were biotinylated and pull downs analysed for CACHD1 and Na⁺/K⁺-ATPase (loading control). In control cells, no immunoreactive CACHD1 was detected, confirming antibody specificity. In CACHD1 expressing cells, immunoreactive CACHD1 was detected. In both cell types, immunoreactive Na⁺/K⁺-ATPase was detected. (C) Cell-surface proteins were biotinylated and pull downs analysed for GFP-Cav3.1-HA (HA) and Na⁺/K⁺-ATPase (loading control). In control cells and cells only expressing CACHD1, no HA signals were detected, confirming antibody specificity. In cells expressing GFP-Cav3.1-HA, HA signals were readily detected. Quantification of the HA signals (normalised to Na⁺/K⁺-ATPase) revealed expression of CACHD1 increased signals for GFP-Cav3.1-HA at the cell-surface, *p<0.05. Na⁺/K⁺-ATPase signals were detected in all

873 cell types (D) Inputs of the biotin pull down assays were analysed by WB. Signals for HA
 874 were only detected in cells expressing GFP-Cav3.1-HA, signals for CACHD1 were only
 875 detected in cells expressing Myc-CACHD1 and signals for β -actin were detected in all cell
 876 types. All blots are representative of $n \geq 3$ experiments.

877

878 **Figure 5. Cav3.1 and CACHD1 are present at the cell-surface and are in close**
 879 **proximity.** Live HEK cells expressing empty vector (vector control, VC), VC + Myc-
 880 CACHD1, GFP-Cav3.1-HA + VC, Myc-CACHD1 + GFP-Cav3.1-HA or CLR•RAMP1
 881 (positive control) were incubated with antibodies to HA and Myc, washed and fixed. (A)
 882 Cells were then incubated with appropriate secondary antibodies and immunoreactive
 883 proteins localised by immunofluorescence and confocal microscopy. In HEK-VC cells, no
 884 signals for GFP, HA or Myc were detected indicating specificity of detection. HA signals
 885 (arrowheads) were only detected in cells expressing GFP-Cav3.1-HA (as determined by the
 886 GFP signal) and CLR•RAMP1. Similarly, Myc signals (yellow arrowheads) were only
 887 detected in cells expressing Myc-CACHD1 and CLR•RAMP1. Scale bar, 10 μ m (B) After
 888 the proximity ligation assay, no signals were detected in cells expressing empty vector or in
 889 cells expressing only Myc-CACHD1 or GFP-Cav3.1-HA. In contrast, PLA signals were
 890 detected in cells expressing Myc-CACHD1 + GFP-Cav3.1-HA (arrows) and CLR•RAMP1
 891 (arrows). Single optical sections are shown except for the PLA panel (CLR•RAMP1
 892 excluded) where 5 optical sections are merged, two above and two below (0.5 μ m
 893 increments) from the optical sections shown in the GFP/DAPI panel. Scale bar, 20 μ m. All
 894 images are representative of $n=3$ experiments. Figure 5 is supported by analysis of cell-
 895 surface CACHD1 construct expression studies (Fig. 5-1).

896

897 **Figure 6. Effects of CACHD1 and $\alpha 2\delta$ -1 on Cav3.1 channels**

898 CACHD1 significantly increased current density as shown by (A) representative current
 899 density traces at -25 mV and (B) I-V relationships, V_H -90 mV (* p <0.05, ** p <0.01,
 900 *** p <0.001, two-way ANOVA with Bonferroni post-hoc test). $\alpha 2\delta$ -1 had no significant
 901 effect on current density as shown by (A) representative current density traces at -25 mV and
 902 (C) I-V relationships, V_H -90 mV. CACHD1, but not $\alpha 2\delta$ -1, significantly increased maximal
 903 conductance (inset, p <0.05, one-way ANOVA with Bonferroni post-hoc test).

904
 905 **Figure 7. Effects of CACHD1 and $\alpha 2\delta$ -1 on Cav3.2 and Cav3.3 channels**

906 CACHD1 significantly increased current density as shown by representative current density
 907 traces at -20 mV for (A) Cav3.2 and (C) Cav3.3, and I-V relationships for (B) Cav3.2 and (D)
 908 Cav3.3; V_H -90 mV (* p <0.05, ** p <0.01, *** p <0.001, two-way ANOVA with Bonferroni
 909 post-hoc test). $\alpha 2\delta$ -1 had no effect on (E) Cav3.2 and (F) Cav3.3 I-V relationships, V_H -90
 910 mV. Figure 7 is supported by analysis of effects of CACHD1 and $\alpha 2\delta$ -1 on Cav3 channel
 911 kinetic properties (Fig. 7-1).

912
 913 **Figure 8. CACHD1 expression increases Cav3.1 gating currents and open probability**
 914 **(Po).**

915 Representative gating currents recorded from Cav3.1 (Aa) and Cav3.1 + CACHD1 (Ab) at
 916 the observed reversal potential. Expanded time scale illustrates the increase in area under the
 917 gating current for CACHD1 expressed cells. B) Conductance vs gating current plot for
 918 multiple cells. Line represents linear regression to data points. The slopes (G_{max}/Q_{max}) were
 919 significantly different ($P=0.0004$, least squares fits compared using extra sum of squares F

test; Cav3.1: 0.09 ± 0.003 , $n=10$, and Cav3.1 + CACHD1: 0.14 ± 0.090 , $n=11$). C) Plot showing the slopes (i.e relative P_o) and S.E.M. for fits shown in B (** $p < 0.001$).

922

923 **Figure 9. Effects of CACHD1 in hippocampal neurons**

924 (A) Co-labelling of hippocampal neurons with CACHD1 and mVenus. (B) CACHD1
925 increased firing frequency of hippocampal neurons. (C) Example traces in response to
926 depolarizing current injections steps of -20, 70 and 140 pA. (D) Summary data from separate
927 experiments confirming CACHD1-mediated increased firing frequency and also showing that
928 TTA-P2 (1 μ M) reduced firing rates in CACHD1-expressing neurons, but not in controls. (E)
929 Rebound APs were evoked using a -50 pA hyperpolarizing prepulse followed by a
930 depolarizing step from 0 pA to 200 pA in steps of 10 pA for 200 ms, CACHD1 expressing
931 neurons displayed a significantly greater number of rebound APs compared to controls. (F)
932 Example traces representing depolarizing current injection steps of 40, 90 and 140 pA. (G)
933 Summary data from separate experiments confirming CACHD1-mediated increased in
934 rebound APs and also showing that TTA-P2 (1 μ M) reduced firing rates in CACHD1-
935 expressing neurons, but not in controls. * $P < 0.05$ throughout, two-tailed paired Student's t-test
936 or one-way ANOVA with Bonferroni post-hoc test. Figure 9 is supported by analysis of
937 effects of CACHD1 and TTA-P2 on biophysical properties of hippocampal neurons (Fig. 9-
938 1).

939

940 **Extended Data Figure Legends**

941

942 **Figure 1-1: CACHD1 mRNA expression in adult rat brain.**

943 *In situ* hybridization of adult rat brain. CACHD1 mRNA was labelled pink with blue
 944 counterstain (Gill's I Haematoxylin). CA1-3: cornus ammonis 1-3; DG: dentate gyrus; g:
 945 granule cell layer; m: molecular layer; p: Purkinje cell; wm: white matter.

946

947 **Figure 1-2: Qualitative expression profile of CACHD1 mRNA and protein in the adult**
 948 **rat brain.**

949 + labelling similar to background; ++ weak labelling; +++ moderate labelling, ++++ strong
 950 labelling; +++++ very strong labelling.

951

952 **Figure 2-1: Expression profile of CACHD1 and voltage-gated calcium channel subunit**
 953 **mRNA in human tissue.**

954 Absolute quantification of CACHD1, $\alpha 2\delta$ -1, -2, -3, Cav2.2 and Cav1, -2, -3 transcripts was
 955 assessed in triplicate by TaqMan® qPCR using 'Best Coverage' Taqman probes (Applied
 956 Biosystems, UK) against a 5-point standard curve of plasmids consisting of 10-fold dilution
 957 of a known copy number of plasmid containing cDNA of the gene of interest. Total RNA was
 958 extracted using an RNeasy kit (Qiagen, UK) with an on-column DNase I treatment.
 959 Additional total RNA samples from AMS Biotechnology (Abingdon, UK) originated from
 960 human male donors aged 24-65.

961

962 **Figure 5-1: Analysis of cell-surface CACHD1 construct expression.**

963 (A, B) HEK cells were transfected with empty vector (vector control, VC) or Myc-CACHD1
 964 and cell lysates analysed by (A) Western blotting (WB) and (B) immunofluorescence and
 965 confocal microscopy. (A) Immunoreactive signals for Myc (mouse Myc, mMyc) were
 966 detected at a similar molecular mass to that predicted for CACHD1 only in cells expressing

967 CACHD1. (B, upper panel) Cells were incubated with antibody to Myc (rabbit Myc, rMyc),
 968 washed, fixed and then incubated with appropriate secondary antibodies. Myc signals
 969 (arrowheads) were only detected in cells expressing Myc-CACHD1. (B, lower panel) Cells
 970 were fixed, incubated with antibody to Myc (rMyc), washed and then incubated with
 971 appropriate secondary antibodies. Myc signals were detected at the cell-surface (arrowheads)
 972 and in intracellular vesicles only in cells expressing Myc-CACHD1. Scale bar, 10 μ m.

973
 974 **Figure 7-1: Effects of CACHD1 and α 2 δ -1 on Cav3 channel kinetic properties**

975 CACHD1 co-expression had no significant effect on $t_{\text{activation}}$ in (Aa) Cav3.1, (Ba) Cav3.2 and
 976 (Ca) Cav3.3. α 2 δ -1 significantly increased Cav3.1 $t_{\text{activation}}$ at all voltages tested (Aa)
 977 (* p <0.05, ** p <0.01, *** p <0.001, two-way ANOVA with Bonferroni post-hoc test); α 2 δ -1
 978 had no effect on Cav3.2 $t_{\text{activation}}$ (Ba); α 2 δ -1 significantly decreased Cav3.3 $t_{\text{activation}}$ at -35
 979 and -30 mV (Ca) (* p <0.05, *** p <0.001, two-way ANOVA with Bonferroni post-hoc test).
 980 CACHD1 co-expression had no significant effect on $t_{\text{inactivation}}$ in (Ab) Cav3.1, (Bb) Cav3.2
 981 and (Cb) Cav3.3. α 2 δ -1 co-expression with Cav3.1 (Ab) resulted in significantly faster
 982 inactivation kinetics (* p <0.05, one-way ANOVA with Bonferroni post-hoc test), but had no
 983 effect on $t_{\text{inactivation}}$ in (Bb) Cav3.2 and (Cb) Cav3.3. Inactivation traces at -20 mV or -30 mV
 984 were fitted with a single exponential function.

985
 986 **Figure 9-1: Effects of CACHD1 and TTA-P2 on biophysical properties of hippocampal**
 987 **neurons.**

988 Extended Data Fig. 9-1 supports Figure 9.

989
 990

991 **Table 1. Effects of CACHD1 and $\alpha 2\delta$ -1 on biophysical properties of Cav3 subtypes.**

	G_{\max} (pS/pF)	$V_{1/2}$ (mV)	k (mV)	τ activation (ms)*	τ inactivation (ms)**
Cav3.1 (18)	628 \pm 70	-34.5 \pm 0.8 (30)	5.4 \pm 0.1 (30)	2.0 \pm 0.1	25.8 \pm 2.0
Cav3.1/ CACHD1 (19)	944 \pm 90*	-36.3 \pm 0.9 (29)	5.6 \pm 0.2 (29)	2.0 \pm 0.2	22.2 \pm 4.8
Cav3.1/ $\alpha 2\delta$-1 (13)	672 \pm 90	-35.7 \pm 1.4	5.6 \pm 0.3	3.3 \pm 0.2 $^{\Delta\Delta}$	18.9 \pm 0.86 $^{\Delta}$
*= $p < 0.05$ vs. Cav3.1 (one-way ANOVA with Bonferroni post-hoc test)					
$^{\Delta}$ = $p < 0.05$, $^{\Delta\Delta}$ = $p < 0.05$ vs. Cav3.1 (two-way ANOVA with Bonferroni post-hoc test)					
Cav3.2 (13)	596 \pm 120	-34.4 \pm 2.4	5.7 \pm 0.2	7.1 \pm 0.40	33.3 \pm 0.97
Cav3.2/ CACHD1 (15)	1060 \pm 140*	-33.4 \pm 0.8	5.9 \pm 0.2	5.9 \pm 0.38	32.0 \pm 1.6
*= $p < 0.05$ vs. Cav3.2 (two-tailed unpaired Student's <i>t</i> -test)					
Cav3.3 (12)	573 \pm 88	-36.1 \pm 1.2	4.3 \pm 0.2	24.4 \pm 1.9	134 \pm 12
Cav3.3/ CACHD1 (10)	849 \pm 78*	-38.9 \pm 1.6	4.0 \pm 0.3	28.5 \pm 3.4	126 \pm 8.3
*= $p < 0.05$ vs. Cav3.3 (two-tailed unpaired Student's <i>t</i> -test)					

992

993 In all cases, comparisons were performed in culture-matched experiments. Numbers in
994 parenthesis represents number of cells each from a minimum of 5 separate transfections.

995

996 * τ activation was measured at -25 mV in all cases.

997 ** τ inactivation was measured at -20 mV for Cav3.1 and Cav3.2 and at -30 mV for Cav3.3.

998

999
1000

Table 2. Effects of CACHD1 and TTA-P2 on hippocampal neuronal firing

	Firing frequency (Hz)	Rebound firing frequency (Hz)
Control	6.0 ± 1.2 (41/6)	7.2 ± 1.2 (32/5)
CACHD1	9.8 ± 1.1* (29/5)	12.1 ± 0.9* (28/5)
Control	8.5 ± 1.4 (6/3)	10.0 ± 1.8 (6/3)
Control + TTA-P2	6.5 ± 1.2 (6/3)	9.2 ± 1.5 (6/3)
CACHD1	14.1 ± 1.7 (7/3)	16.7 ± 0.8 (10/3)
CACHD1 + TTA-P2	6.9 ± 1.4* (7/3)	10.0 ± 1.2* (10/3)
*= p<0.05 vs control two-tailed paired Student's <i>t</i> -test		
Values represent means ± S.E.M; number in parenthesis = number of neurons/number of separate transfections.		

1001
1002

1003

Figure 1. Cottrell et al

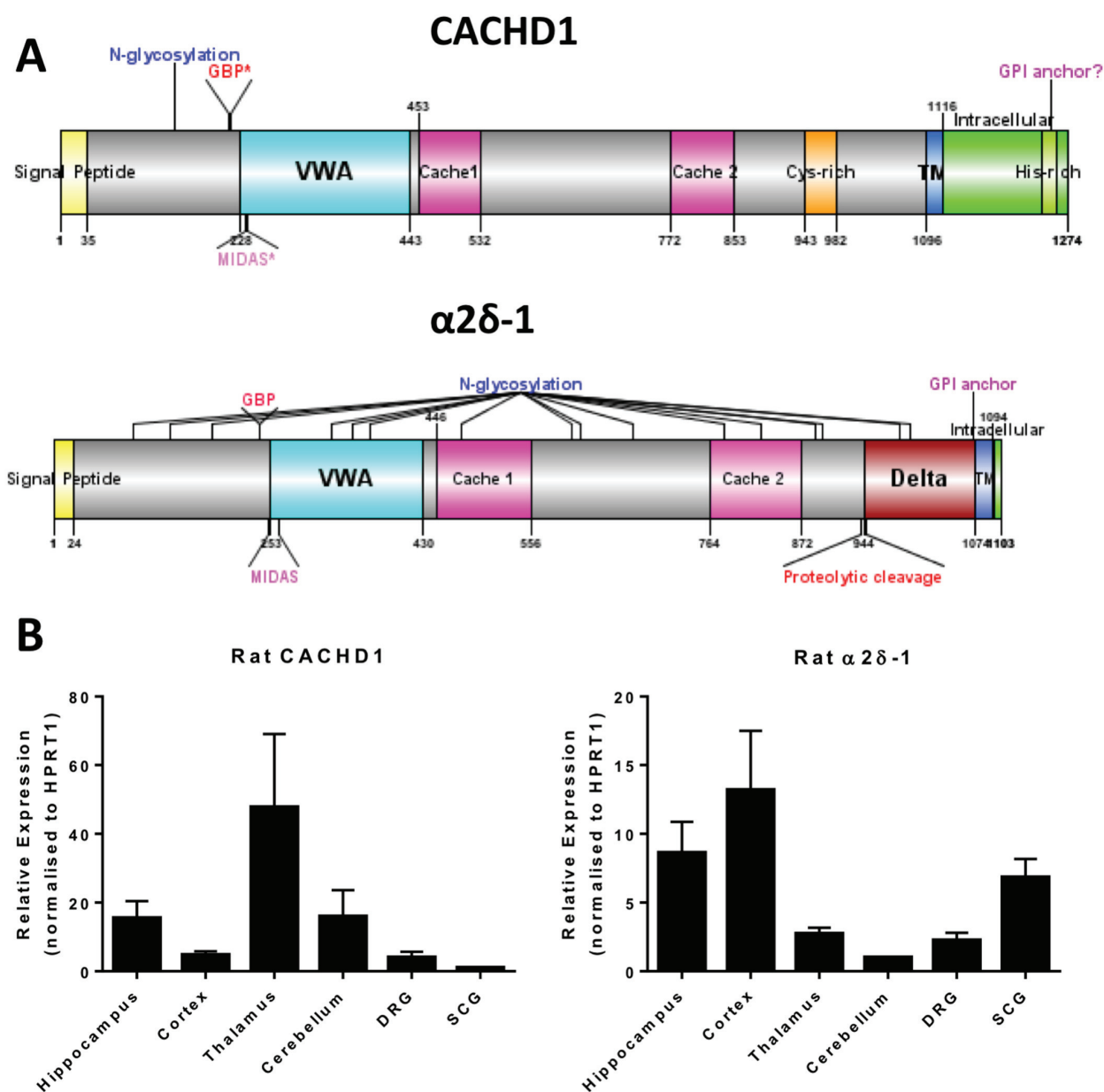


Figure 2. Cottrell et al

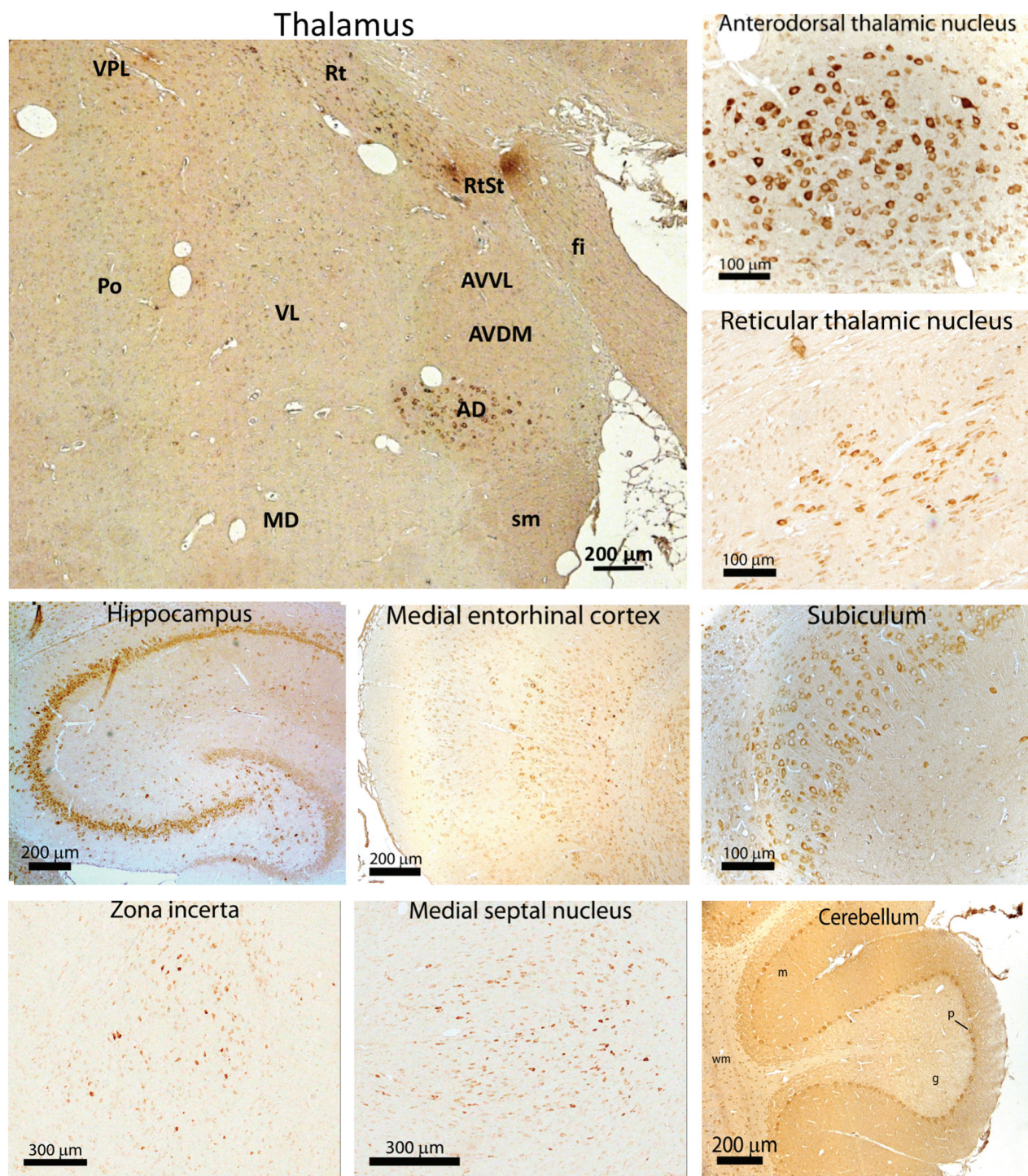
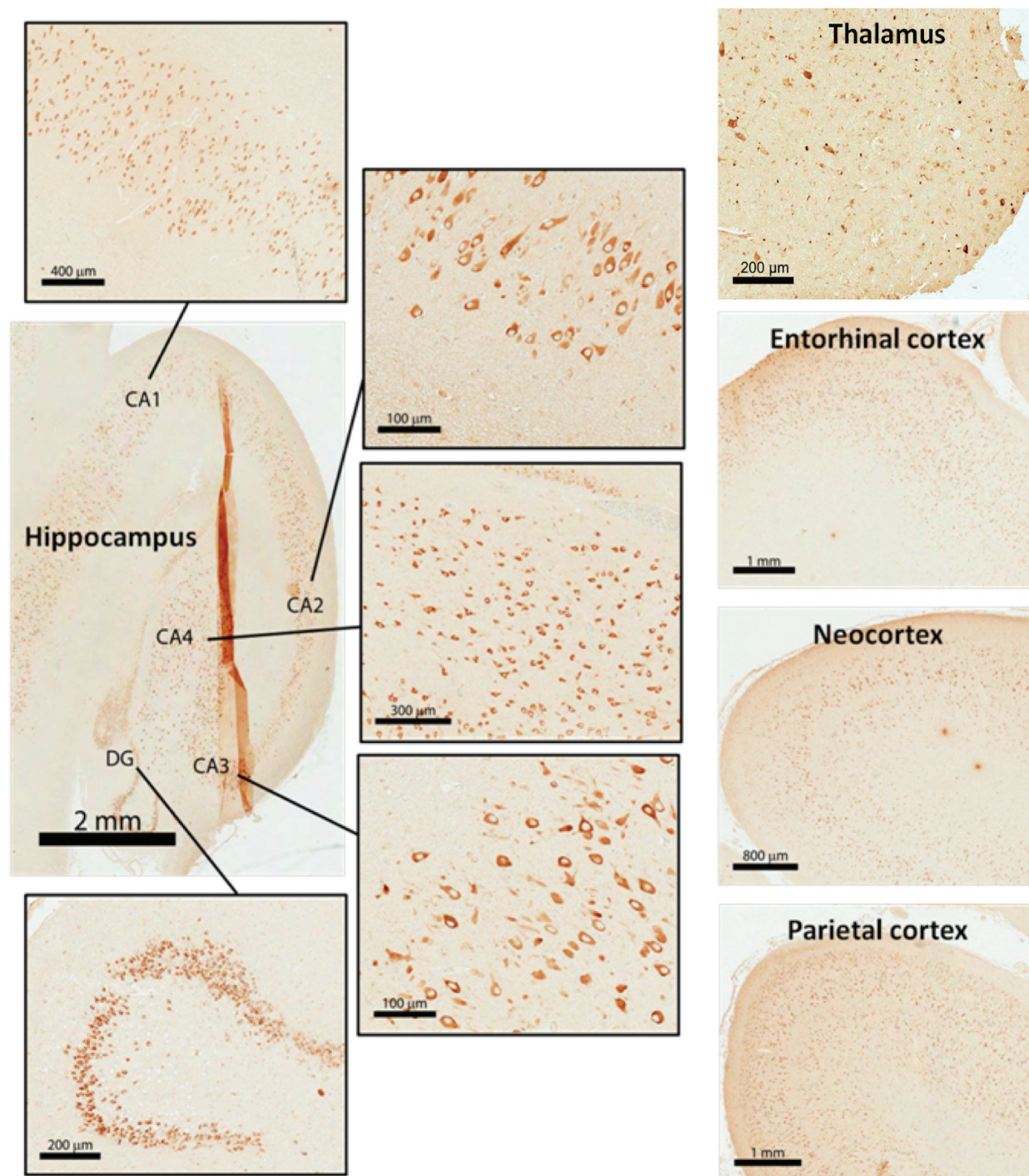
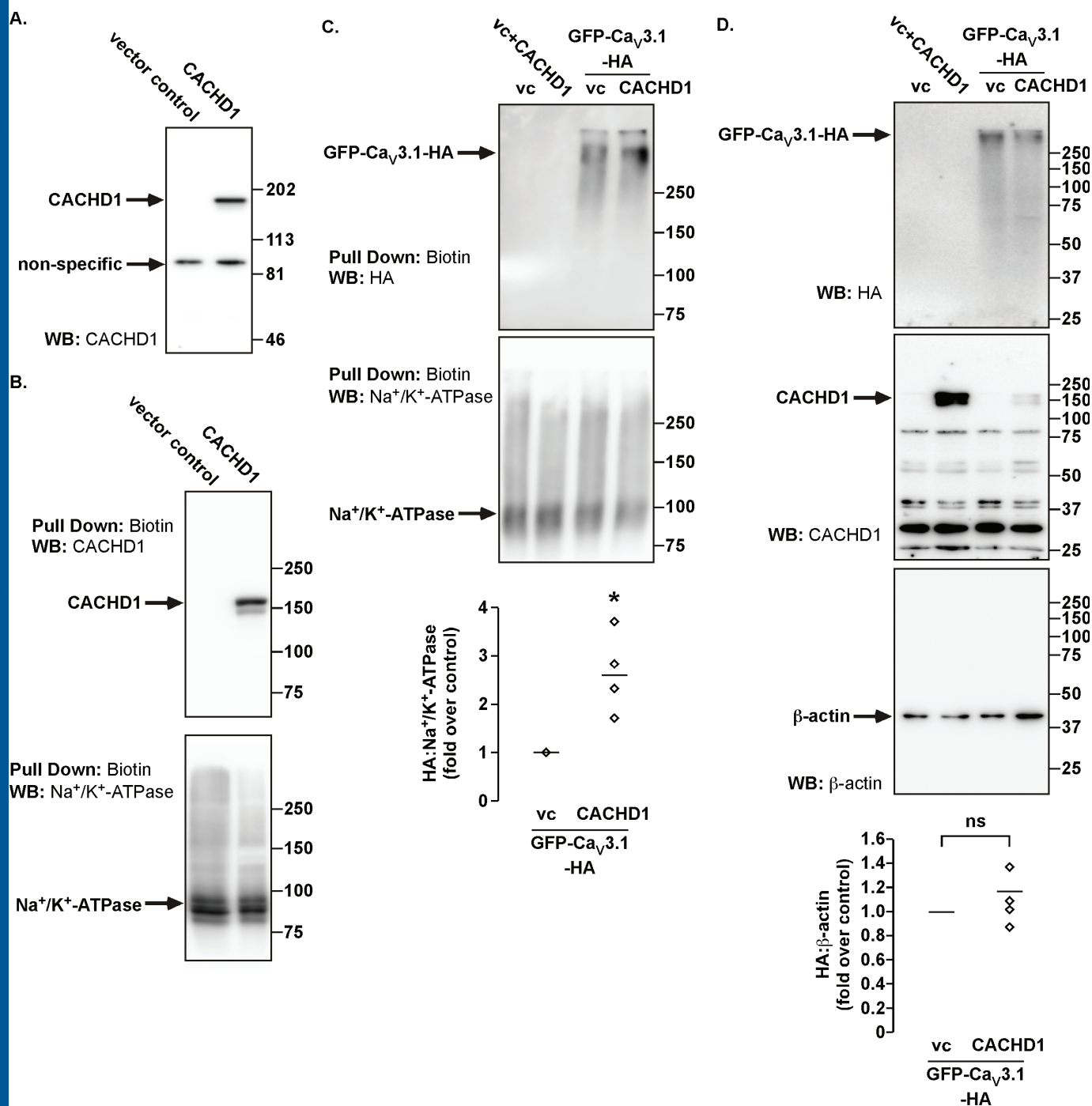


Figure 3. Cottrell et al





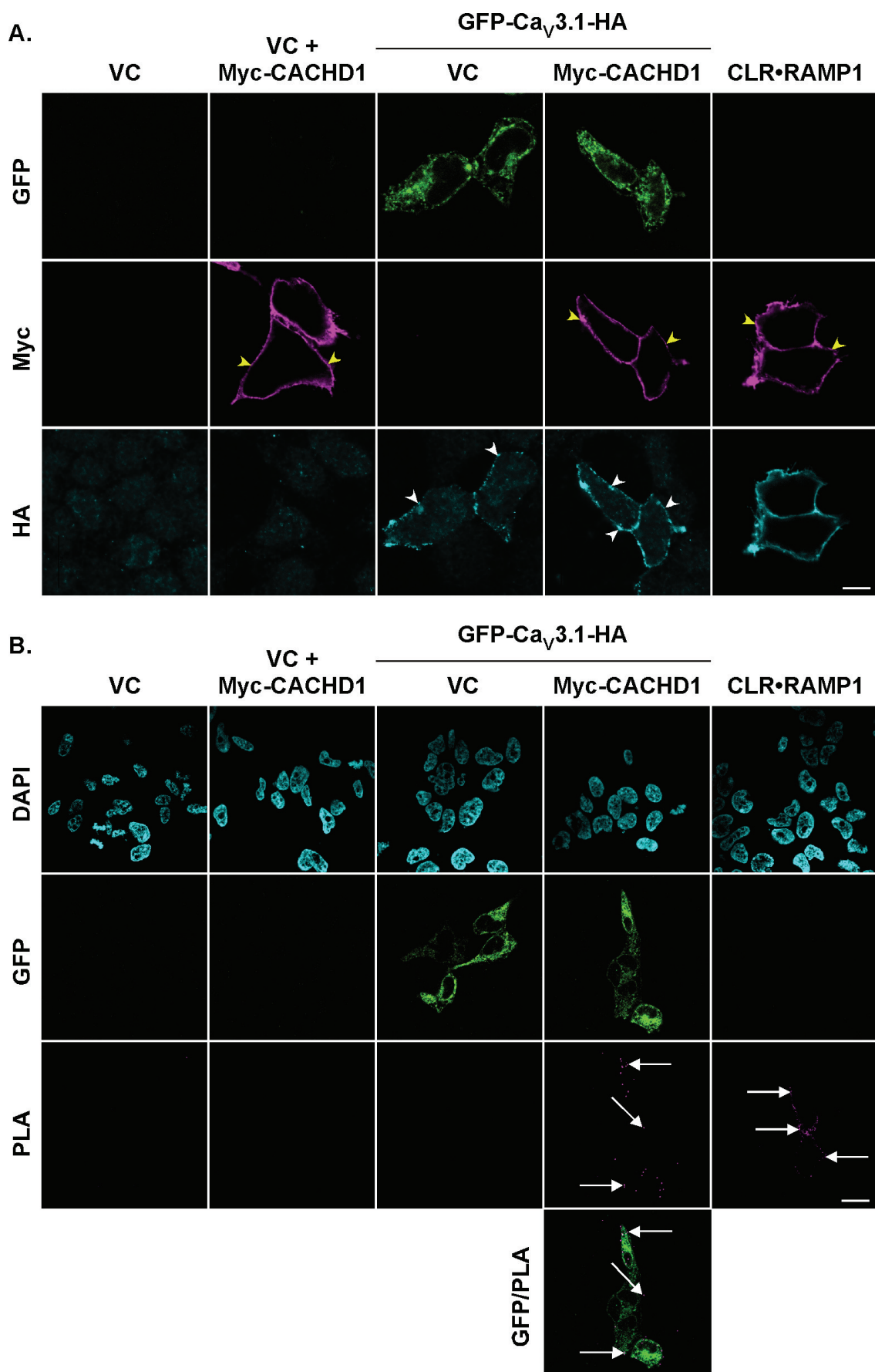


Figure 6. Cottrell et al

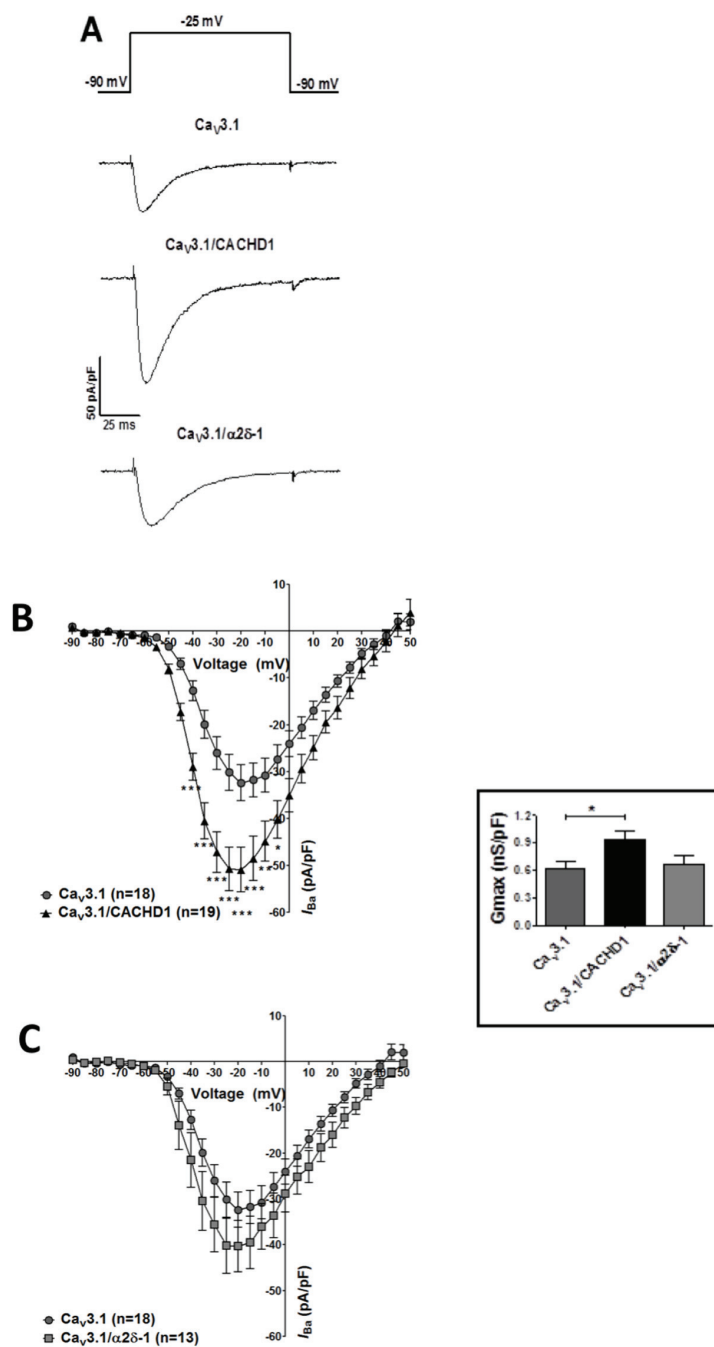


Figure 7. Cottrell et al

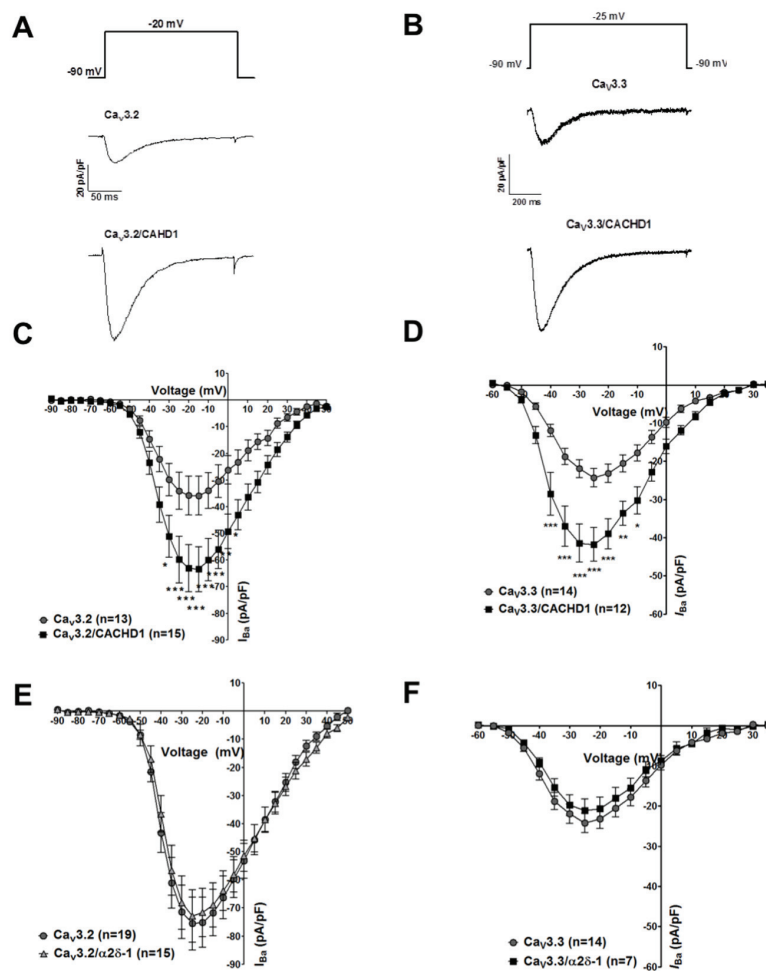


Figure 8. Cottrell et al

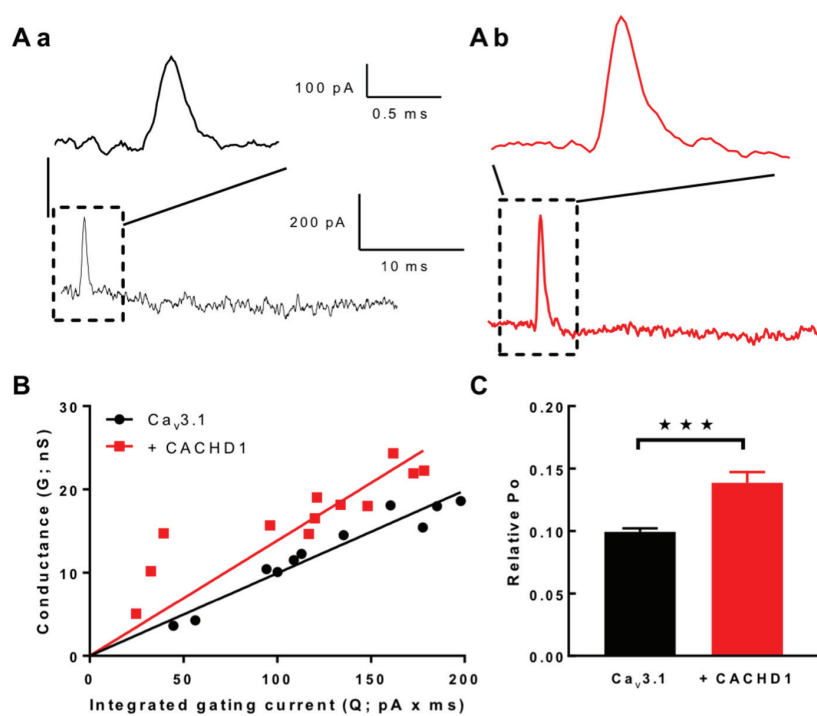


Figure 9. Cottrell et al

